Lithos 302–303 (2018) 126–141

Contents lists available at ScienceDirect

Lithos

journal homepage: www.elsevier.com/locate/lithos

Role of deep-Earth water cycling in the growth and evolution of continental crust: Constraints from Cretaceous magmatism in southeast China

Zhen Li [a,b,c,*], Xuan-Ce Wang [a,c,*], Simon A. Wilde [a], Liang Liu [d], Wu-Xian Li [e], Xuemei Yang [a]

[a] The Institute for Geoscience Research (TIGeR), Department of Applied Geology, Curtin University, GPO Box U1987, Perth, WA 6845, Australia
[b] State Key Laboratory of Petroleum Resources and Prospecting, China University of Petroleum, Beijing 102249, PR China
[c] The School of Earth Science and Resources, Chang'an University, Xi'an 710054, PR China
[d] State Key Laboratory of Ore Deposit Geochemistry, Institute of Geochemistry, Chinese Academy of Sciences, Guiyang 550081, PR China
[e] State Key Laboratory of Isotope Geochemistry, Guangzhou Institute of Geochemistry, Chinese Academy of Sciences, Guangzhou 510640, PR China

ARTICLE INFO

Article history:
Received 4 November 2017
Accepted 28 December 2017
Available online 3 January 2018

Keywords:
Southeast China
Cretaceous magmatism
Deep-Earth water cycling
Water-fluxed melting
Continental crustal growth

ABSTRACT

The late Mesozoic igneous province in southeast China provides an excellent opportunity to understand the processes that controlled the growth and evolution of Phanerozoic continental crust. Here we report petrological, whole-rock geochemical and isotopic data, and *in situ* zircon U–Pb–Lu–Hf isotopic data from granitoids and associated gabbros in the Pingtan and Tong'an complexes, southeast China. Through combining the new results with published datasets in southeast China, we show that the Early Cretaceous magmatic rocks are dominated by juvenile Nd–Hf isotopic compositions, whereas the Late Cretaceous ones display less radiogenic Nd–Hf isotope signatures. Furthermore, Nd–Hf isotope systematics are coupled with decreasing abundance of hydrous minerals and an increase of zircon saturation temperatures. Compiled zircon Hf–O data indicates that the 117–116 Ma granites have zircon $\delta^{18}O$ values ranging from mantle values (close to 5.3‰) to as low as 3.9‰, but with dominantly positive initial epsilon Hf ($\varepsilon_{Hf}(t)$) values. Zircon grains from 105 to 98 Ma rocks have $\delta^{18}O$ values plotting within the mantle-like range (6.5‰ − 4.5‰), but mainly with negative $\varepsilon_{Hf}(t)$ values. Zircon grains from ca. 87 Ma rocks have positive $\varepsilon_{Hf}(t)$ values (+9.8 to +0.7) and a large range of $\delta^{18}O$ values (6.3‰ − 3.5‰). The variations in Hf–Nd–O isotopic compositions are correlated with decreasing abundance of magma water contents, presenting a case that water-fluxed melting generated large-scale granitic magmatism. Deep-Earth water cycling provides an alternative or additional mechanism to supply volatiles (e.g., H_2O) for hydrous basaltic underplating, continental crustal melting, and magmatic differentiation.

1. Introduction

Continental crust covers about 40% of the Earth's current surface (Cogley, 1984). Its growth and evolution have influenced the global lithosphere, hydrosphere, and atmosphere, and have generated a biologically unique environment (Taylor and McLennan, 1995). Granitic batholiths and their erupted counterparts, a major component of upper continental crust, bear vital information on the generation and secular evolution of the continents that was controlled by Earth's geodynamic systems, such as crust–mantle interaction and differentiation, and tectonic-plate recycling (Taylor and McLennan, 1995). Granite, used *sensu lato* here, is a common type of felsic intrusive igneous rock that is granular and phaneritic in texture, consisting of the felsic minerals quartz, feldspar, and subordinate mica and amphibole (Best, 2013). Chemical and isotopic compositions of most granites preclude their direct mantle origin, making them a principal agent of crustal differentiation (Taylor and McLennan, 1995). However, some granitoids display juvenile radiogenic isotopic signatures (e.g., Sr–Nd–Hf; Chen et al., 2014; Griffin et al., 2002; Kemp et al., 2009) and mantle-like oxygen (O) (e.g., Chen et al., 2014), especially those formed at long-lived convergent plate boundaries (e.g., subduction zones and active continental margins). Such isotopic signatures suggest a juvenile input to these granites and possibly reflect mantle contributions in their generation, and have been utilized to identify continental crustal growth (here meaning the addition of mantle-derived material to the continental crust) (e.g., Hawkesworth et al., 2010; Kemp et al., 2009). If this implies a direct mantle origin, then a high proportion of mantle input (30%–90%) is required regardless of the isotopic system used (e.g., whole-rock Sr–Nd, zircon Lu–Hf, or zircon O isotopes; Hawkesworth et al., 2010; Liu et al., 2013). Such a high proportion of mantle input is inconsistent with the

* Corresponding authors at: Department of Applied Geology, Curtin University, GPO Box U1987, Perth, WA 6845, Australia.
E-mail addresses: zhen.li@curtin.edu.au (Z. Li), x.wang3@curtin.edu.au (X.-C. Wang).

https://doi.org/10.1016/j.lithos.2017.12.028
0024-4937/

major element composition of granites and basaltic mantle-derived melts (Taylor and McLennan, 1995), and does not correlate with the felsic-dominant rock associations with only minor basaltic rocks found at many convergent plate boundaries (e.g., eastern China and eastern Australia; Kemp et al., 2009; X.M. Zhou et al., 2006). In contrast, it has been argued that granites with apparently juvenile radiogenic isotopic compositions can be derived by partial melting of juvenile lower crust (Jahn et al., 2000). Consequently, the origin of the juvenile radiogenic and mantle-like O isotopic characteristics of these granites remains controversial, and this in turn hampers our ability to determine the processes that controlled continental crustal growth and its evolution throughout Earth history.

Another commonly held view is that granitic magmatism is essentially linked to the presence of abundant water on Earth (e.g., Campbell and Taylor, 1983). Previous models for generating the parental magmas attributed supply of the necessary water mainly to dehydration reactions due to breakdown of muscovite/biotite/amphibole (Miller et al., 2003, and references therein), and regarded dehydration melting, with the absence of a separate aqueous phase, as a key process that produced large volumes of granitic magmas (e.g., Clemens and Watkins, 2001). In contrast, other researchers emphasized that water-fluxed melting involving a free H_2O phase could produce the complexities in chemical composition and field relationships between different melt phases seen in some granitic belts (Brown, 2001; Weinberg and Hasalová, 2015; Whitney, 1988). The latter view is further supported by investigations of granitic magmatism in the North China Craton (Ma et al., 2016), and in the United States and New Zealand Cordillera (Collins et al., 2016). However, more studies are required to ascertain where the water was located that drove crustal melting. Furthermore, it remains unclear whether or not, and by what mechanisms, water-fluxed melting can control the rich variety of granitoids found at the local to regional scales. These issues are relevant to understanding how important water-fluxed melting is in driving continental crustal growth.

The mantle transition zone (MTZ), between the 410 km and 660 km seismic discontinuities, has been considered as a crucial water reservoir in the Earth's interior (e.g., Kuritani et al., 2011; Niu, 2014; Wang et al., 2015, and references therein). Increasing evidence from geochemical, geophysical, global tectonic, mantle convection, and thermochemical modelling studies indicates the importance of the hydrated MTZ in driving Earth's geodynamic system (Kuritani et al., 2011; Wang et al., 2015). Recent studies combining oxygen isotopes with conventional geochemistry of global continental flood basalts suggest that dehydration of stagnant slabs within the MTZ can result in wet upwelling of mantle materials rooted atop or within the MTZ and these will then hydrate the lowest part of the continental lithosphere and generate hydrous basaltic melts (Wang et al., 2015, 2016). A > 4000 km long corridor of synchronous, isotopically similar mid-Cretaceous kimberlite magmatism in central North America suggests water-fluxed decompression melting of C-O-H-bearing peridotite in the MTZ to account for their OIB (ocean island basalts) type deep mantle source (Kjarsgaard et al., 2017). Ponding of hydrous melts and fluids at the lithosphere-asthenosphere boundary could then act as a lubricant to speed-up plate motion and breakup of supercontinents (Wang et al., 2015). This is further evidenced by a recently identified pervasive low seismic velocity layer above the MTZ beneath the western US (Hier-Majumder and Tauzin, 2017). The high estimated water contents (4.82 ± 1.00 wt%) in primitive basaltic rocks from the Tarim large igneous province (Xia et al., 2016) also suggest a hydrous origin for some continental flood basalts. These results link deep-Earth water cycling, large-scale intra-continental magmatism and supercontinent cycles into a self-organized system (Wang et al., 2015, 2016). Moreover, Tang et al. (2016) compiled global geochemical data for Archean shales, glacial diamictites, and igneous rocks, to track the bulk MgO composition of the Archean upper continental crust. Their results demonstrated a five-fold increase in the mass of the Archean upper continental crust due to the rise of voluminous felsic magmatism that produced the tonalite–trondhjemite–granodiorite rocks (TTGs). Recent phase equilibrium modelling further demonstrated that Archean TTGs could be produced by partial melting of highly hydrated basalts/metabasic rocks (Johnson et al., 2017). Thus, the deep-Earth water cycling process and its potential links with geodynamic processes would not only provide a fresh perspective for answering some fundamental questions about granite petrogenesis, such as where could the fluid be derived from and the exact role of water in producing granitic melts, but may also enable us to identify the geodynamic processes for the growth and evolution of TTG continental crust on the early Earth.

Here we present petrological, whole-rock and isotopic geochemical, and *in situ* zircon U–Pb–Hf–O isotopic data for Cretaceous plutonic rocks in Fujian Province, southeast (SE) China. We use these data to investigate the exact nature of the juvenile isotopic features of these granitoids, and to argue for the key role played by water-fluxed melting in producing large-scale granitic magmatism. Based on contrasting geological signatures for the Early and Late Cretaceous granites in Fujian Province, and observations of regional tectono-magmatic evolution, we advocate the possible linkage between deep-Earth water cycling and continental crustal growth and its evolution through time.

2. Geological setting

SE China, located at the western Pacific margin, is an important part of the circum-Pacific magmatic belt. The late Mesozoic geodynamic setting in SE China is interpreted as an active continental margin related to the subduction of the Paleo-Pacific Plate beneath the East Asian continent (Li et al., 2014, and references therein). Late Mesozoic magmatism in SE China formed a > 200,000 km^2 large igneous province dominantly composed of felsic rocks, with a subordinate mafic component (Chen et al., 2008). More than 68% of the intermediate to acidic rocks here were generated during the Cretaceous (ca. 145–66 Ma; X.M. Zhou et al., 2006), and are restricted to a narrow zone along the coastal region, known as the Southeast Coast Magmatic Belt (SCMB; Fig. 1a; Chen et al., 2008). The Cretaceous felsic rocks here consist mainly of calc-alkaline granitic batholiths and volcanic–intrusive complexes with relatively juvenile isotopic compositions (X.M. Zhou et al., 2006), that have been related to the subduction of the Paleo-Pacific plate (Li et al., 2014). In addition, evidence from geophysical surveys in East Asia (Huang and Zhao, 2006), systematic investigations of Cenozoic volcanism in northeast China (Kuritani et al., 2011; Wang et al., 2015), and geodynamic studies on the delamination/thinning mechanisms of the sub-continental lithospheric mantle (SCLM) of the North China Craton (Windley et al., 2010), indicate that the deeply subducted and stagnant Pacific slab beneath East Asia extends horizontally beneath the hinterland over a distance of 800 to >1000 km, and that this may be responsible for the intensive hydration of the MTZ beneath eastern China (Wang et al., 2015).

The distinctive geological setting makes Cretaceous igneous activity in SE China an excellent example to determine the petrogenesis of granites with juvenile radiogenic isotope compositions, and to unravel the possible linkage between deep-Earth water cycling and continental crustal growth. As shown in Fig. 1, the coastal area of Fujian has the best exposures of undeformed Cretaceous granites within the entire SCMB, representing a microcosm of Cretaceous felsic magmatism in SE China. The main igneous intrusions along the Fujian coast are composed of I-type granitoids with compositions ranging from granodiorite to alkali-feldspar granite, and which were followed by local Late Cretaceous highly-evolved A-type granites (X.M. Zhou et al., 2006). Small volumes of Early Cretaceous mafic intrusions (<5% of the total volume of Fujian igneous rocks) are dominantly gabbroic, crop out sporadically, and are spatially related to the contemporaneous granitoids (Li et al., 2014).

3. General geology and petrography of the Pingtan and Tong'an complexes

The Pingtan complex is well exposed on Pingtan Island in east Fujian Province, and is the fifth largest island in China with an area of 323 km^2

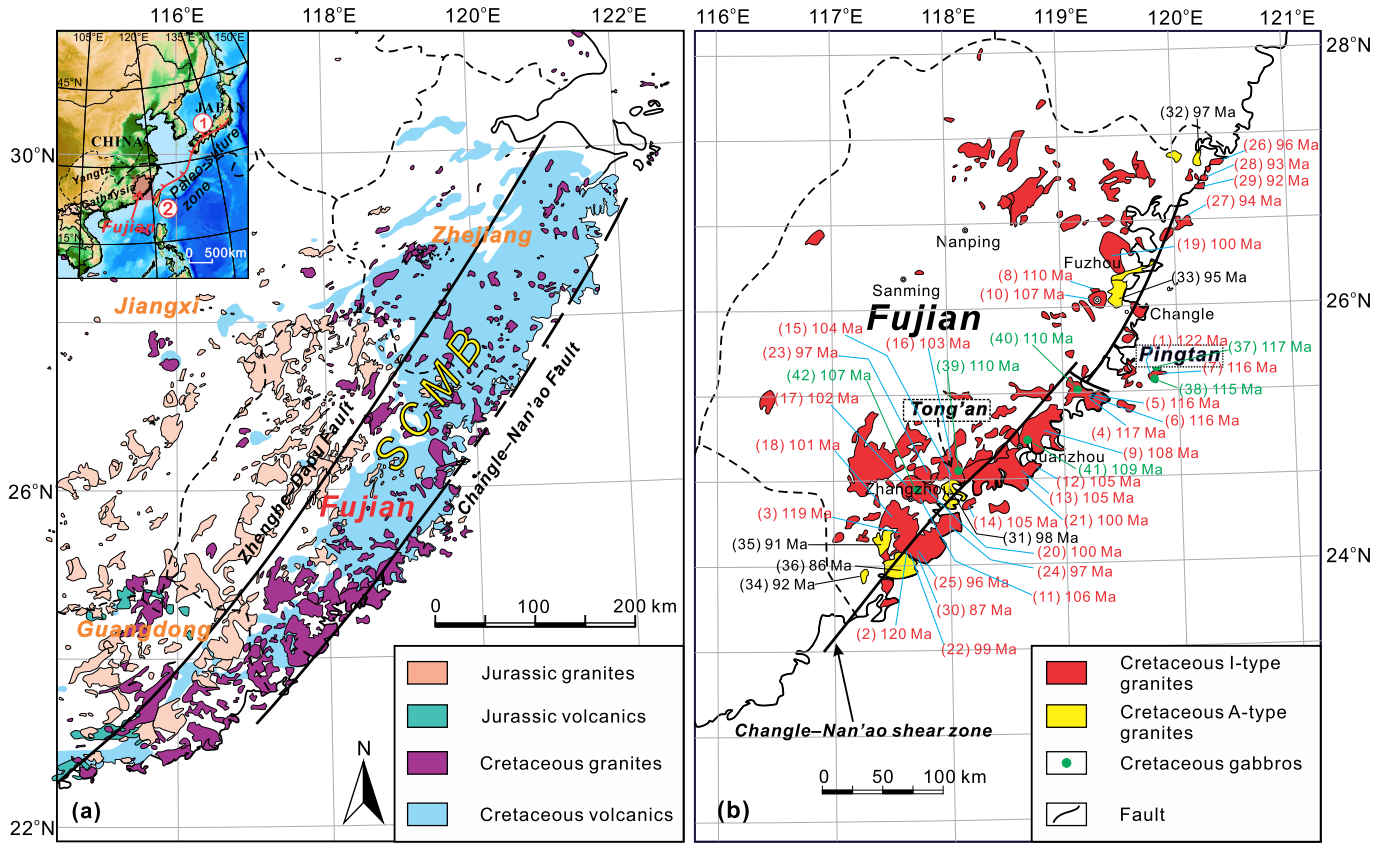

Fig. 1. (a) Generalized geological map showing the distribution of late Mesozoic granites and volcanics in the SE China coastal region (modified after X.M. Zhou et al., 2006). Inset figure shows a simplified tectonic map of SE China with a speculated paleo-suture zone of the Paleo-Pacific slab in the late Mesozoic (modified after Li et al., 2014). Numbers 1 and 2 in the inset figure represent the Median Tectonic Line in Japan and the eastern flank of the Central Ranges in Taiwan, China, respectively. SCMB denotes the Southeast Coast Magmatic Belt. (b) Simplified geological map of the Fujian coastal area showing the distribution and ages of the Cretaceous batholiths as tabulated in Table B.2 (modified after Li et al., 2014).

(Figs. 1b and 2a) (X. Xu et al., 1999). The intrusive rocks are composed mainly of biotite monzogranite and biotite syenogranite, with minor amphibole-bearing gabbro, and intruded into volcanic rocks of the Lower Cretaceous Shimaoshan Formation. Some rocks show complicated field characteristics resulting from mixing of mafic and felsic magmas (e.g., microgranular enclaves, mutual intrusive relations, and synplutonic dikes) (X. Xu et al., 1999). The amphibole-bearing gabbros are distributed mainly in the central part of the complex (Fig. 2a), and are medium- to coarse-grained with the main minerals being subhedral to euhedral plagioclase (~60%), amphibole (15%–35%) and clinopyroxene (5%–15%) (Fig. A.1a). Amphibole-bearing gabbros with less amphibole (PT-1) come from a small stock located in the southeastern part of Pingtan Island (Fig. 2a), containing plagioclase (55%–60%), clinopyroxene (20%–35%) and amphibole (5%–8%), with minor hypersthene (Figs A.1b and 1c). They have a cumulate texture consisting of plagioclase and clinopyroxene (Fig. A.1b). The granitic intrusions form the outer part of the complex and are mainly made up of biotite monzogranite and biotite syenogranite with massive, medium- to coarse-grained allotriomorphic-granular textures. Granodioritic microgranular enclaves are present in some biotite syenogranites. The biotite monzogranites contain alkali feldspar (~35%), quartz (~35%), plagioclase (20%–25%) and biotite (5–10%), with accessory Fe–Ti oxides (including magnetite) and zircon (Fig. A.1d). The major minerals in biotite syenogranite are alkali feldspar (35%–40%), quartz (30%–40%), plagioclase (10–15%) and biotite (5%–10%) (Fig. A.1e). Accessory minerals include Fe–Ti oxides, apatite, and zircon. The granodioritic microgranular enclaves are spheroidal to ellipsoidal in shape with no evidence of deformation, and range in size from several to a dozen centimeters. They generally have a fine-grained microgranular texture, consisting mainly of plagioclase (~60%), alkali feldspar (~20%), quartz (10%–15%), and minor biotite (~5%) (Fig. A.1f). In addition, euhedral acicular apatite generally occurs as an accessory mineral in the microgranular enclaves (Fig. A.1f), indicative of rapid cooling and crystallization (e.g., Vernon et al., 1988).

The Tong'an complex is a bimodal plutonic complex cropping out in the northwestern suburbs of Tong'an in southeastern Fujian Province (Fig. 1b). Locally, amphibole-bearing gabbros are exposed as pod-like bodies that intruded into volcanic rocks of the Lower Cretaceous Nanyuan Formation and coexist with biotite granodiorites (Fig. 2b). The gabbros consist mainly of plagioclase (~55%), amphibole (30%–40%), clinopyroxene (5%–10%) and minor biotite (0%–3%) (Figs. A.2a and 2b). The rocks display a hypidiomorphic texture with clinopyroxene locally enclosed by plagioclase and amphibole. Amphibole, the most abundant mafic mineral in the Tong'an gabbro, occurs mainly as subhedral to euhedral megacrysts and locally as poikilitic crystals, and is locally altered to chlorite (Figs. A.2a and 2b). Biotite granodiorite is the dominant rock-type in the Tong'an complex (Fig. 2b), and is massive and medium- to coarse-grained with the major minerals being plagioclase (~50%), quartz (~25%), alkali feldspar (~15%) and biotite (~10%) (Figs. A.2c and 2d). Accessory phases include magnetite and zircon. The plagioclase is euhedral–subhedral and generally shows polysynthetic twinning and compositional zoning. Neither microgranular enclaves nor mingling structures are found in the Tong'an complex.

4. Sampling and analytical methods

We collected 14 fresh samples as being representative of the two Cretaceous intrusive complexes, with lithologies ranging from gabbro to granite (see Fig. 2 for sample locations). For the Pingtan complex, samples were collected from amphibole-bearing gabbro (PT-1, PT-2,

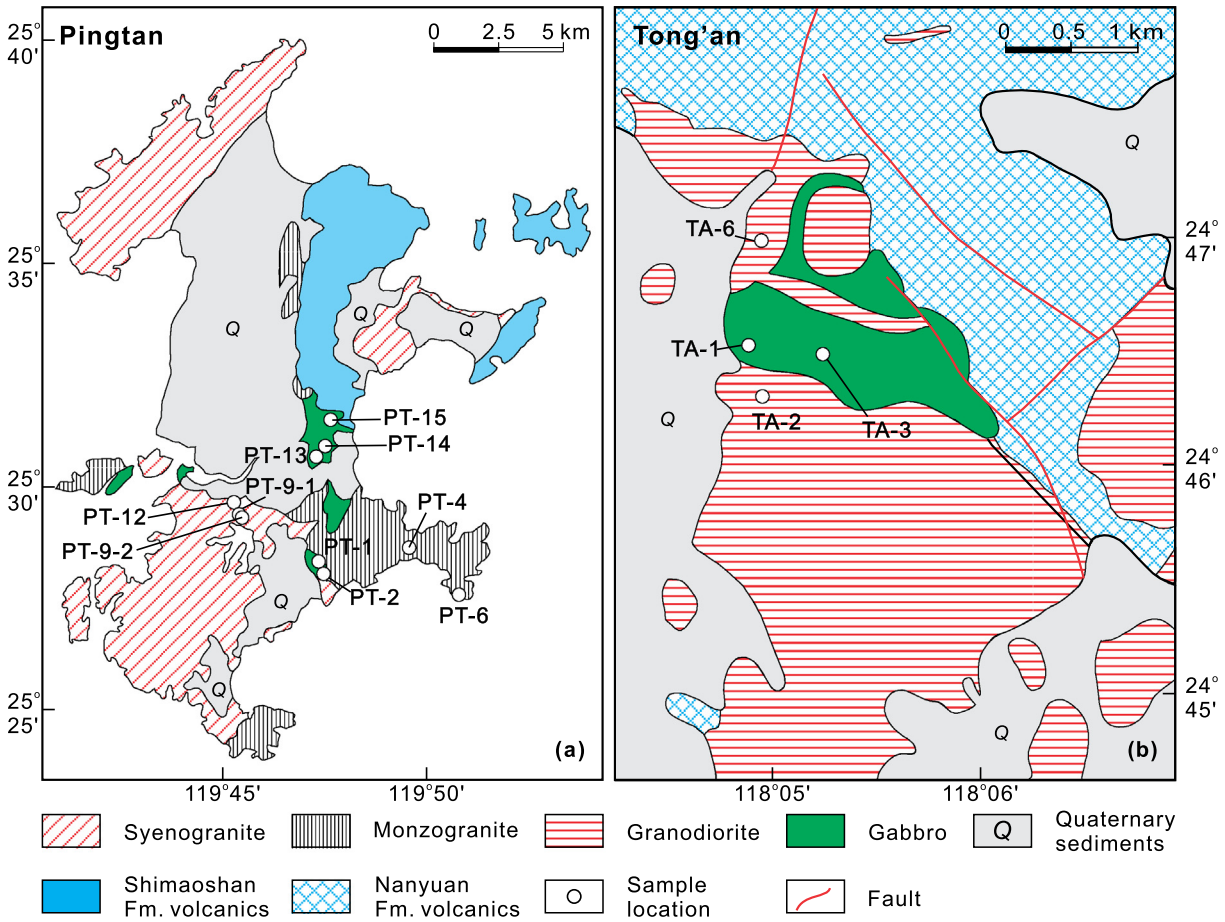

Fig. 2. (a) Geological sketch map of the Pingtan complex in the Fujian coastal area (modified from the 1:500,000 geological map of Fujian Province, Bureau of Geology and Mineral Resources of Fujian Province, 1998). (b) Geological sketch map of the Tong'an complex in the Fujian coastal area (modified after Li et al., 2012). Both maps show the sample locations.

PT-13, PT-14, and PT-15), biotite monzogranite (PT-4 and PT-6), biotite syenogranite (PT-12 and PT-9-1), and a granodioritic enclave (PT-9-2) in biotite syenogranite. For the Tong'an complex, samples were obtained from amphibole-bearing gabbro (TA-1 and TA-3) and biotite granodiorite (TA-2 and TA-6). The whole-rock geochemical compositions of all these samples were determined, along with the Sr–Nd isotopic compositions of a subset of 12 samples. Eight of the samples were prepared for zircon U–Pb dating in order to constrain the emplacement ages of these rocks, and seven of the dated samples were also analyzed for *in situ* zircon Lu–Hf isotopes. We then integrated our new data with a compilation of petrological, geochronological, and geochemical data for 36 contemporaneous intrusions (mainly granitoids) from Fujian Province (Tables B.1–B.4 and Fig. 1b) to test the role of water in the generation of the Cretaceous plutonic rocks. Details of analytical procedures and results are provided in Appendices A and B.

5. Results

5.1. Zircon U–Pb geochronology

Zircon grains from the Pingtan and Tong'an complexes generally exhibit typical magmatic oscillatory zoning in CL images (Figs. 3f and 4d). The results of *in situ* U–Pb dating are presented in Table A.1 and shown in Figs. 3–4. Zircon grains from the amphibole-bearing gabbros (samples PT-1 and PT-14) in the Pingtan complex record U–Pb weighted mean ages of 115 ± 1 Ma and 117 ± 3 Ma, respectively (Figs. 3a–3b). Zircon grains from the biotite monzogranite (sample PT-6) and biotite syenogranite (sample PT-9-1) have $^{206}Pb/^{238}U$ ages of 116 ± 2 Ma and 122 ± 2 Ma, respectively (Figs. 3c–3d). A granodioritic enclave (sample PT-9-2) within the Pingtan biotite syenogranite has a zircon $^{206}Pb/^{238}U$ age of 124 ± 2 Ma (Fig. 3e), which is interpreted to represent its crystallization age, coeval with the host granite.

The amphibole-bearing gabbro (sample TA-3) from the Tong'an complex has a crystallization age of 110 ± 1 Ma and two samples of the biotite granodiorite (TA-2 and TA-6) record $^{206}Pb/^{238}U$ ages of 101 ± 1 Ma and 103 ± 1 Ma, respectively (Fig. 4). These results confirm that the mafic and felsic intrusions within each of the complexes have broadly similar Early Cretaceous emplacement ages, but that the Tong'an complex is younger.

5.2. Whole-rock major and trace element compositions

The whole-rock major and trace element data are presented in Table A.2 and shown in Figs 5, 6a–6d, and A.3. The gabbros in both complexes are mainly subalkaline in composition with a calc-alkaline signature (Figs. 5a–5b). The Pingtan gabbros have SiO_2 contents of 46.96–51.51 wt%, whereas the Tong'an samples record values of 43.18–45.59 wt%. Both are characterized by moderately-enriched light rare earth elements (LREEs) with $(La/Yb)_N$ ratios of 8.7–10.0 (Pingtan) and 8.0–12.5 (Tong'an) and small positive to weakly negative Eu anomalies, with Eu/Eu^* values of 1.03–1.21 (Pingtan) and 0.89–1.07 (Tong'an) (Table A.2 and Figs. 6a–6b). In primitive mantle-normalized trace element spidergrams (Figs. 6c–6d), the gabbros display enrichment in large ion lithophile elements (LILEs; Rb, Ba, Th, U, and K) and depletion in high field strength elements (HFSEs; Nb and Ta), similar to the trace element patterns of typical arc magmatic rocks. The Pingtan granites

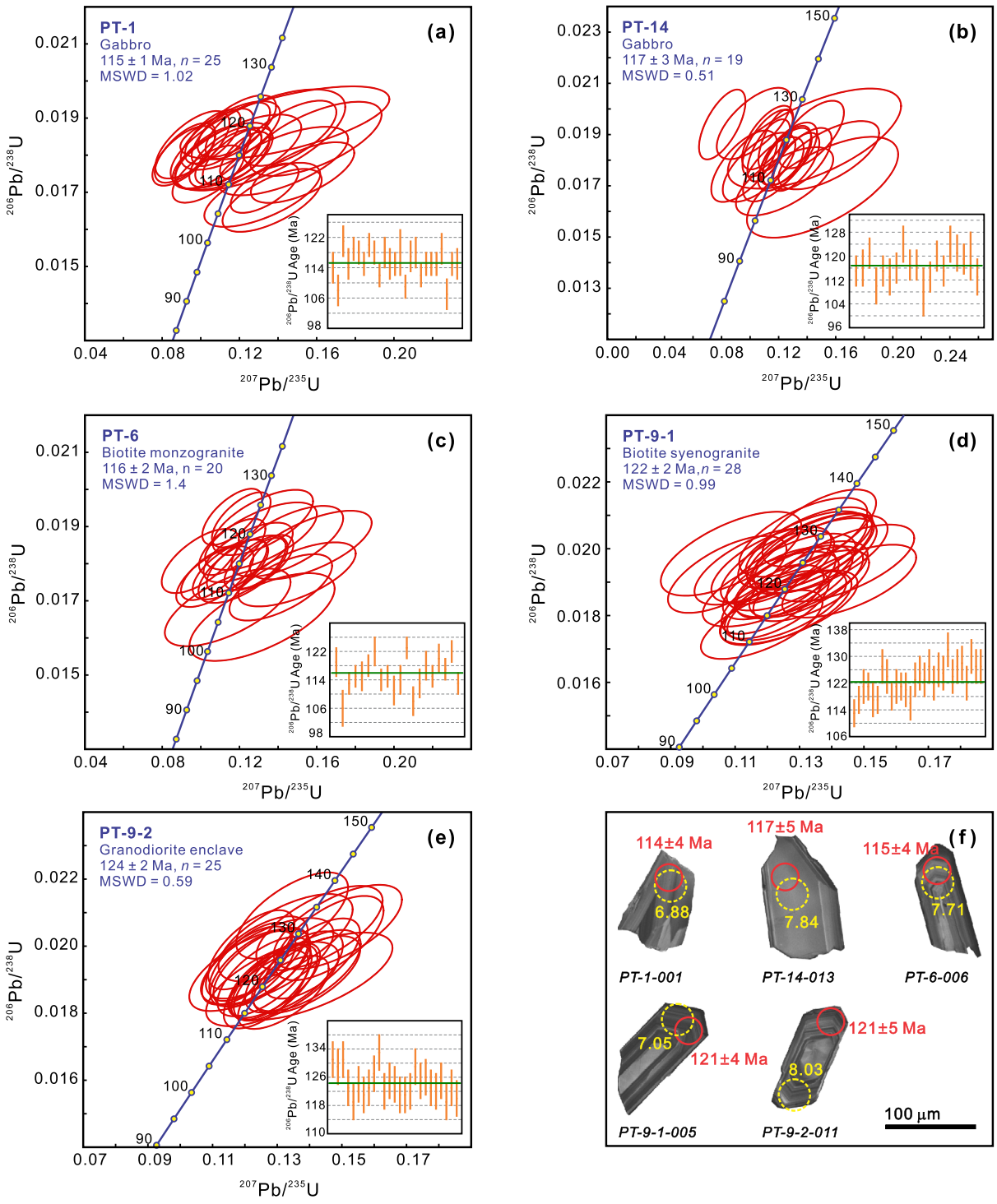

Fig. 3. Zircon U–Pb concordia diagrams for samples of the Pingtan complex in the Fujian coastal area: (a) PT-1, gabbro; (b) PT-14, gabbro; (c) PT-6, biotite monzogranite; (d) PT-9-1, biotite syenogranite; and (e) PT-9-2, granodioritic microgranular enclave in biotite syenogranite. (f) Representative zircon CL images of the Pingtan igneous rocks. The small red solid circles indicate the U–Pb dating sites, and the large yellow dashed circles indicate the positions of Lu–Hf isotopic analyses. The U–Pb age and $\varepsilon_{Hf}(t)$ values are shown for each zircon.

(monzogranites, syenogranites, and granodiorite enclave) include both calc-alkaline and high-K calc-alkaline types, whereas the Tong'an granodiorites generally have a high-K calc-alkaline signature (Figs. 5a–5b). These rocks are typical I-type granitoids with low A/CNK (molar $A1_2O_3/(CaO + Na_2O + K_2O)$) values of 0.97–0.99 (Pingtan) and 0.98–0.99 (Tong'an) (Table A.2 and Fig. 5c), and show bimodal major element characteristics with the coexisting gabbros on Harker diagrams (Fig. A.3). The granitoids differ from the gabbros in terms of moderate to weak negative Eu anomalies, with Eu/Eu* values of 0.65–0.96 (Pingtan) and 0.84–0.86 (Tong'an) (Table A.2 and Figs. 6a–6b), and by being strongly enriched in Pb and depleted in Ti (Figs. 6c–6d). However, they exhibit remarkable similarities in rare earth element (REE) patterns and contents and trace element spidergrams to the coexisting gabbros, including moderate enrichment in LREEs, with $(La/Yb)_N$ ratios of 9.6–14.4 (Pingtan) and 18.9–20.6 (Tong'an), and enrichment in Rb, Th, U, and K and depletion of Nb and Ta (Figs. 6a–6d).

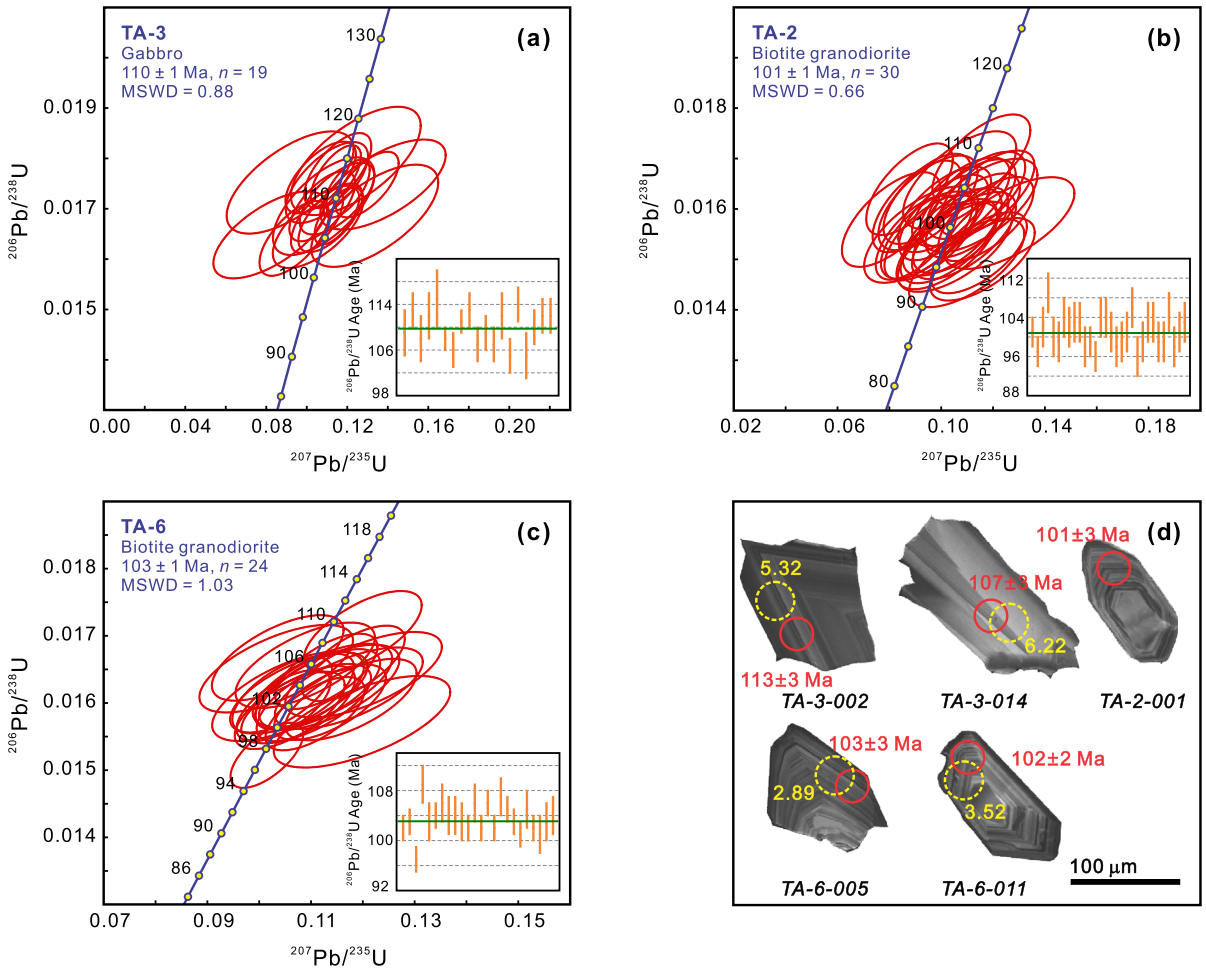

Fig. 4. Zircon U–Pb concordia diagrams for samples of the Tong'an complex in the Fujian coastal area: (a) TA-3, gabbro; (b) TA-2, biotite granodiorite; and (c) TA-6, biotite granodiorite. (d) Representative zircon CL images of the Tong'an igneous rocks. The small red solid circles indicate the U–Pb dating sites, and the large yellow dashed circles indicate the positions of Lu–Hf isotopic analyses. The U–Pb age and $\varepsilon_{Hf}(t)$ values are shown for each zircon.

5.3. Whole-rock Sr–Nd isotopes

The whole-rock Sr–Nd isotopic compositions are summarized in Table A.3 and displayed in Fig. 6e and f. The Pingtan gabbros exhibit fairly uniform initial $^{87}Sr/^{86}Sr$ ratios (0.705357 to 0.705396) and $\varepsilon_{Nd}(t)$ values (−0.4 to −1.0), comparable to the granitoids which have $^{87}Sr/^{86}Sr$ ratios of 0.705472 to 0.705672 (with the exception of PT-12 with a value of 0.707700) and $\varepsilon_{Nd}(t)$ values of −0.7 to −1.7 (Table A.3). The granodioritic enclave (sample PT-9-2) in the Pingtan biotite syenogranite displays similar Sr–Nd isotope signatures to its host granite, with initial $^{87}Sr/^{86}Sr$ ratio of 0.705610 and $\varepsilon_{Nd}(t)$ value of −0.4 (Table A.3 and Figs. 6e–6f).

Likewise, the gabbros and granodiorites in the Tong'an complex possess consistent Sr and Nd isotopic features, with initial $^{87}Sr/^{86}Sr$ ratios of 0.705845 to 0.706152 (Tong'an gabbros) and 0.706017 to 0.706094 (Tong'an granodiorites), and $\varepsilon_{Nd}(t)$ values of −2.8 to −3.8 (Tong'an gabbros) and −2.8 to −3.5 (Tong'an granodiorites) (Table A.3).

5.4. Zircon Lu–Hf isotopes

The results of *in situ* zircon Lu–Hf isotope analyses are presented in Table A.4 and shown in Fig. 7. Rocks from the two complexes and the granodiorite enclave in the Pingtan syenogranite have juvenile zircon Lu–Hf isotopic compositions (Fig. 7). The Pingtan gabbros have $\varepsilon_{Hf}(t)$ values of +13.0 to +1.1, similar to the Pingtan granitoids, with $\varepsilon_{Hf}(t)$ values ranging from +10.6 to −1.2, and to the granodiorite enclave in the Pingtan biotite syenogranite, with $\varepsilon_{Hf}(t)$ values ranging from +10.9 to +0.4. The Tong'an gabbros and granitoids also reveal similar zircon Hf isotope compositions, with $\varepsilon_{Hf}(t)$ = +6.2 to +1.0 and +4.0 to −0.2, respectively (Table A.4), but differ from the Pingtan rocks in being less radiogenic.

6. Discussion

6.1. Petrogenesis of the Pingtan and Tong'an complexes: crust-mantle interaction and water-fluxed melting

The relationship between the granitoids and gabbros in the Pingtan and Tong'an complexes has been revealed by their close temporal and spatial distributions, and their similar trace elemental and isotopic signatures (Figs. 2–4, and 6–7). A prominent characteristic of the granitoids and granodioritic enclaves (occurring in some granitoids of the Pingtan complex) is their juvenile zircon Lu–Hf isotopic compositions, with $\varepsilon_{Hf}(t)$ values of +10.6 to −1.2 (Pingtan granite), +10.9 to +0.4 (Pingtan granodiorite enclave), and +4.0 to −0.2 (Tong'an granodiorite) (Table A.4 and Fig. 7). Furthermore, the samples also have $\varepsilon_{Nd}(t)$ values of −0.7 to −1.7 (Pingtan granite), −0.4 (Pingtan granodiorite enclave), and −2.8 to −3.5 (Tong'an granodiorite) (Table A.3), much less negative than those of basement metamorphic rocks in SE China. As shown in

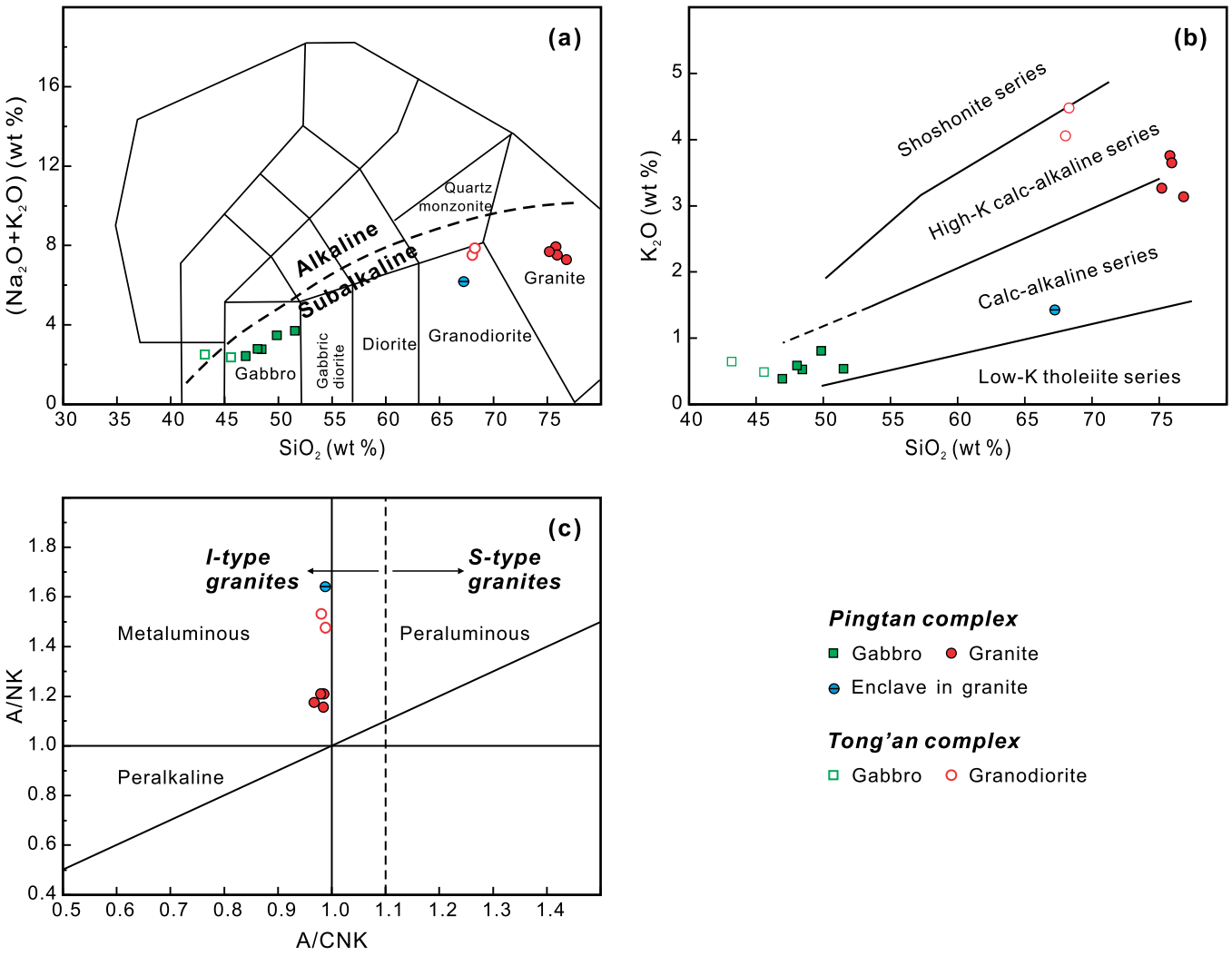

Fig. 5. (a) Total alkali–silica (TAS) diagram for samples from the Pingtan and Tong'an complexes in the Fujian coastal area (modified after Middlemost, 1994). The boundary between alkaline and subalkaline series is after Irvine and Baragar (1971). (b) K_2O vs. SiO_2 diagram for samples from the Pingtan and Tong'an complexes in the Fujian coastal area. The series boundaries are after Peccerillo and Taylor (1976). (c) A/NK (molar $Al_2O_3/(Na_2O + K_2O)$) vs. A/CNK (molar $A1_2O_3/(CaO + Na_2O + K_2O)$) diagram for granitoid samples from the Pingtan and Tong'an complexes in the Fujian coastal area (modified after Chappell and White, 1974; Maniar and Piccoli, 1989).

Fig. 6e, the Nd isotopes of the granitoids plot above the evolutionary trend defined by the Proterozoic crust of the South China Block and close to the CHUR (chondritic uniform reservoir) reference line.

These lines of evidence reflect the involvement of a large proportion of juvenile components in the genesis of these granitoids, so the synchronous and spatial distribution of mafic and felsic rocks in these complexes seem to corroborate that crust-mantle interaction was involved in their generation. The mixed (crust and mantle) origin of these igneous complexes is supported by the presence of gabbro/diorite/granodiorite enclaves within some granitoids of the Pingtan complex (Griffin et al., 2002; X. Xu et al., 1999; this study), and the presence of mutual intrusive relations and synplutonic dikes (Griffin et al., 2002). In addition, magma mixing seems to be able to account for the Hf isotopic heterogeneity of magmatic zircon grains from the Pingtan and Tong'an granitoids (Table A.4 and Fig. 7) (Griffin et al., 2002). It may thus be deduced that mixing of crustal melts with mantle-derived materials played an essential role in the generation of these granitoids, like the previously-envisaged scenario for some other Mesozoic magmatic rocks in northeast China (e.g., Yang et al., 2007), and SE China (e.g., Griffin et al., 2002; Liu et al., 2013). However, such inferences can be challenged.

Firstly, the mass balance based on binary mixing calculations between typical depleted mantle-derived melts (represented by the late Mesozoic alkaline basalts from Hunan in South China; Li et al., 2004) and supracrustal materials (represented by typical S-type granites, the Darongshan S-type granites in south China; Hsieh et al., 2008) using the Sr–Nd isotopic data suggests >60% and 51% direct mantle input is required in the source of the Pingtan and Tong'an granitoids, respectively (Fig. 6f). Such an extremely high proportion of mantle input contrasts with their high silica contents (SiO_2 = 68.0–76.8 wt%) and depletion of incompatible elements (MgO = 0.41–1.22 wt%, Cr = 3–23 ppm, Ni = 0.51–8.84 ppm) (Table A.2). Furthermore, field evidence for magma mixing (e.g., mafic enclaves, mutual intrusive relations, and synplutonic dikes, etc.) was only observed in the Pingtan complex, whereas no such evidence was found in any other gabbro–granite complexes along the Fujian coastal area (including the Tong'an, Daiqianshan, Qinglanshan, and Quanzhou complexes; Li et al., 2012; this study).

Secondly, the zircon Hf isotope compositions of coexisting mafic and felsic rocks preclude the possibility of producing the felsic end-member by mixing processes as required by the two-end member mixing model. As shown in Fig. 7, the mafic and felsic rocks have similar zircon Hf

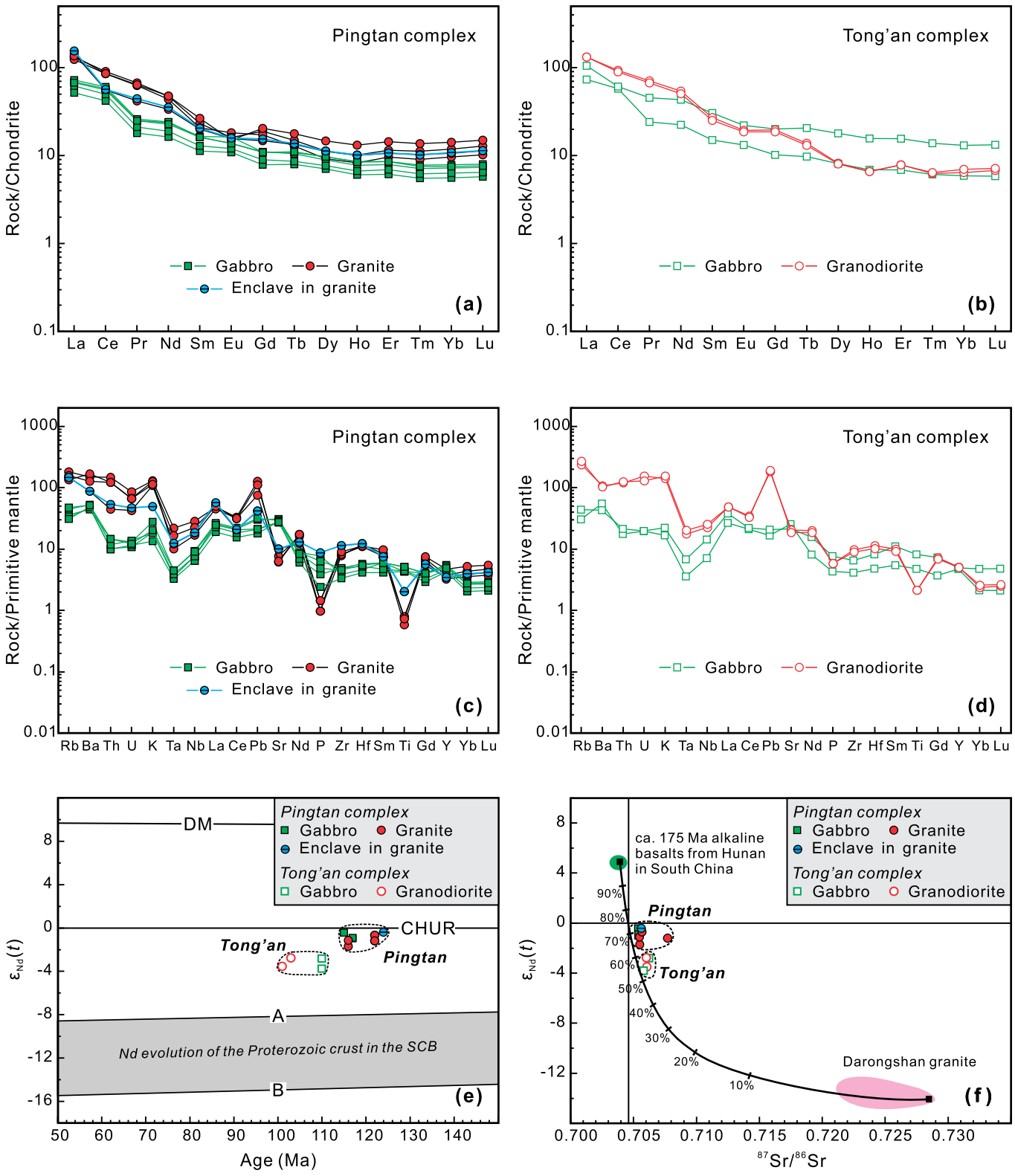

Fig. 6. (a–b) Chondrite-normalized REE patterns and (c–d) primitive mantle-normalized trace element spidergrams for samples from the Pingtan and Tong'an complexes, respectively, in the Fujian coastal area. Normalized values for chondrite and primitive mantle are from McDonough and Sun (1995). (e) $\varepsilon_{Nd}(t)$ vs. age diagram for samples from the Pingtan and Tong'an complexes. DM, depleted mantle; CHUR, chondritic uniform reservoir. Line A represents the Proterozoic crustal end-member of higher degree of maturation in the South China Block, with average isotopic compositions of $^{147}Sm/^{144}Nd = 0.1198$ and $^{143}Nd/^{144}Nd = 0.511822$; line B represents the Proterozoic crustal end-member of lower degree of maturation in the South China Block, with average isotopic compositions of $^{147}Sm/^{144}Nd = 0.1246$ and $^{143}Nd/^{144}Nd = 0.512170$ (Shen et al., 1993). (f) Initial $\varepsilon_{Nd}(t)$ vs. $^{87}Sr/^{86}Sr$ diagram for samples from the Pingtan and Tong'an complexes. The binary mixing curve between possible mafic and felsic magma end-members was constructed using a depleted mantle composition represented by the late Mesozoic alkaline basalts from Hunan in South China (Li et al., 2004) and a crustal end-member represented by the Darongshan S-type granite (Hsieh et al., 2008). Tick marks show 10% mixing increments.

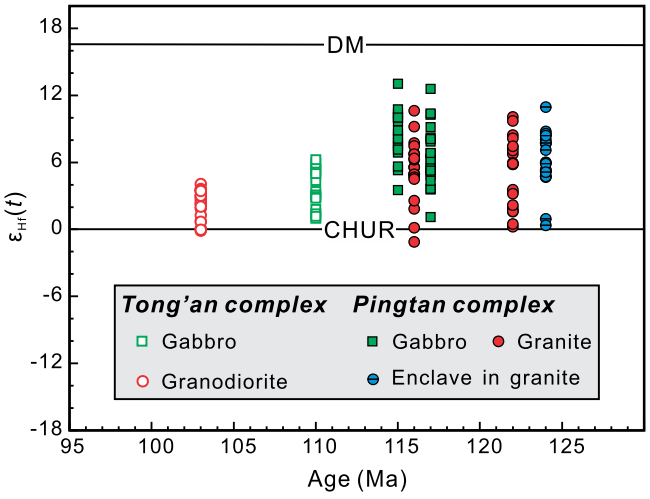

Fig. 7. Zircon $\varepsilon_{Hf}(t)$ vs. U–Pb age diagram for samples from the Pingtan and Tong'an complexes. DM, depleted mantle; CHUR, chondritic uniform reservoir.

isotopes, with the $\varepsilon_{Hf}(t)$ values spread over a range of +13.0 to +1.1 for the Pingtan gabbros, and +10.6 to −1.2 for the Pingtan granites. Likewise, the spread is +6.2 to +1.0 for the Tong'an gabbros and +4.0 to −0.2 for the Tong'an granodiorite (Table A.4). The distinct lack of zircon grains with $\varepsilon_{Hf}(t) << 0$ in these granitoids argues against significant involvement of pre-existing evolved crustal components (such as supracrustal material) in the generation of the felsic end-member. Instead, the highly heterogeneous zircon $\varepsilon_{Hf}(t)$ values within single specimens from the Pingtan and Tong'an granitoids (Fig. 7) can be explained by incongruent/disequilibrium crustal melting as an alternative to the mixing between mantle-derived mafic magmas and crustal-derived felsic magmas (Tang et al., 2014), especially considering the lack of clear field evidence for magma mixing in the Tong'an complex, and the younger ages of the Tong'an granodiorites compared to the gabbros.

Taken together, there is no evidence for massive mantle input and it alone cannot directly account for the juvenile radiogenic isotope signature of the granitoids in both complexes. A more feasible mechanism is therefore required to produce the juvenile isotopic features of the felsic end-member of these two complexes. Partial melting of juvenile lower crust heated up by magma underplating could explain the co-existence of juvenile radiogenic isotopic signatures and high silica contents in the Pingtan and Tong'an granitoids (Jahn et al., 2000). Late Mesozoic basaltic underplating in SE China has been indicated by evidence from geophysical, petrogenetic, and metamorphic investigations. This includes the presence of late Mesozoic gabbroic granulite xenoliths in Cenozoic breccia pipes (X.S. Xu et al., 1999), reverse Vp values at the crust-mantle transition zone (Wang et al., 1993), high Poisson's ratios that reflect an intermediate to mafic composition of the crust (Xia et al., 2015), and high Cretaceous geothermal gradients (Chen et al., 2008). However, numerical simulations of heat transfer (e.g., Petford and Gallagher, 2001) imply that underplating of basaltic magmas at the base of continental crust cannot provide sufficient heat to extensively melt the mafic lower crust. Even if the lower crust is amphibolite, basaltic underplating alone cannot be the dominant mechanism to produce large-scale partial melting of lower continental crust due to the high dehydration-melting temperature of amphiboles in mafic rocks (about 950 °C). However, this paradox can be solved if the generation of granitic melts involved fluids (e.g., Collins et al., 2016).

Gabbros from these complexes contain ubiquitous hydrous minerals, with 5%–35% and 30%–40% amphibole in the Pingtan and Tong'an gabbros, respectively (Table B.2 and Figs. A.1–A.2). The high proportion of hydrous minerals in these gabbros suggests significant water contents in their parental magmas. The plagioclases from the Pingtan and Tong'an gabbros are characterized by high anorthite components, with average anorthite contents ranging from 85% to 86% in Pingtan (X. Xu et al., 1999), and from 90% to 95% in Tong'an (Li et al., 2012). The presence of anorthitic plagioclase is also a typical characteristic of parental magmas with high water contents (Waters and Lange, 2015). Moreover, the mafic mineral assemblage in these gabbros is dominated by amphibole, with the percentage ranging from about 50% to 88% in Pingtan, and from about 75% to 89% in Tong'an (Table B.2 and Figs. A.1–A.2), whereas orthopyroxene is almost absent in the gabbros. This most likely suggests a crystallization environment with >5 wt% water content in the melts (Chen et al., 2016, and references therein). The above lines of evidence suggest that the inferred parental magmas of these gabbros were most likely hydrous. Furthermore, the Pingtan and Tong'an granitoids have low zircon saturation temperatures of 670–706 °C (Table A.2), analogous to those observed in water-fluxed crustal melting in the Cordilleran batholiths (Collins et al., 2016). We thus propose that underplating of hydrous basaltic magmas not only provided a mechanism to produce mafic end-members in the Pingtan and Tong'an complexes, but also released H_2O and possibly other hydrous fluids from underplated basaltic rocks. Similar to "Water-fluxed crustal melting" (Collins et al., 2016; Weinberg and Hasalová, 2015; Whitney, 1988), underplating by hydrous basaltic rocks provides a possible mechanism to supply heat and, more importantly, free H_2O to promote partial melting of juvenile continental crust in order to generate the felsic end-members of the Pingtan and Tong'an complexes. Although mixing between underplated hydrous mafic magmas and felsic melts may occur and account for mingling structures and gabbro-diorite-granodiorite enclaves in the Pingtan granites (Griffin et al., 2002; X. Xu et al., 1999; this study), our first-order interpretation is that water-fluxed melting played a key role in producing the Pingtan and Tong'an granites with juvenile radiogenic isotope compositions, and may provide a new perspective for deciphering the processes involved in continental crustal growth.

6.2. Secular changes of magma H_2O contents and Hf–Nd–O isotopes of the Cretaceous granites in Fujian

The majority of Cretaceous I- and A-type granites in Fujian Province are calc-alkaline to high-K calc-alkaline in composition, and are bimodal with the broadly coeval gabbros, a typical characteristic of back-arc extensional magmatism induced by subduction of the Paleo-Pacific slab (Li et al., 2014). These granites are generally enriched in LREEs and LILEs (Rb, Th, U, and K), and show variable depletion of Nb and Ta, similar to the coexisting gabbros, but all granites exhibit negative Eu anomalies and variable depletion in Ba, Sr, P, and Ti (Fig. A.4). Although the enrichment of LREEs and LILEs and depletion of HFSEs (Nb and Ta) are generally regarded as the characteristics of island-arc melts, these arc-like geochemical signatures can also be produced by deep-Earth water cycling in a non-arc environment (Wang et al., 2016).

Data from the Pingtan and Tong'an complexes, together with the available plutonic magmatic database for Fujian Province, define a linear NNE–SSW trending belt of Cretaceous plutonism (Fig. 1). Such a linear trend was thought to be a response to subduction of the Paleo-Pacific plate beneath eastern China (Li et al., 2014), where Cretaceous intrusions are dominantly I-type granites that formed between 122 and 87 Ma (Table B.2 and Fig. 8). Subordinate Late Cretaceous A-type granites were emplaced between 98 and 86 Ma, and most are spatially associated with the I-type granites (Fig. 1b). Minor gabbroic intrusions formed in the interval between 117 and 107 Ma. These latter closely resemble gabbros in the Pingtan and Tong'an complexes, and are predominantly amphibole-bearing gabbros that temporally and spatially coexist with the I-type granites (Table B.2 and Fig. 1b).

Detailed petrographic and geochemical examination highlights pivotal differences between the Early Cretaceous and Late Cretaceous granitoids, demonstrating a decrease in water content within the parental magmas over time. The Early Cretaceous I-type granites generally contain

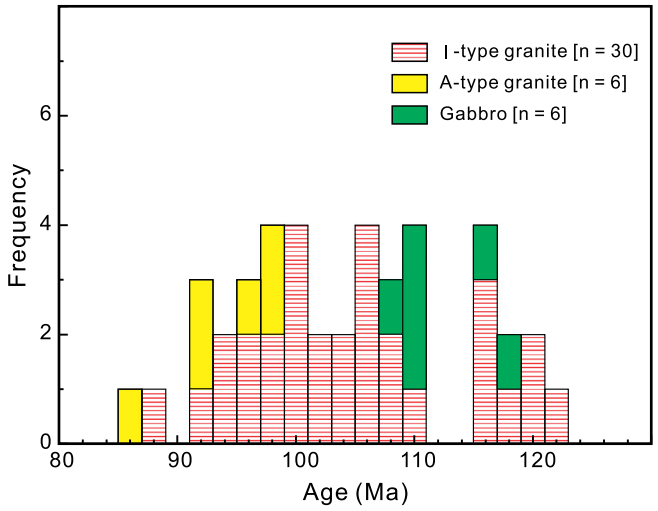

Fig. 8. Frequency distribution of ages of Cretaceous plutons of various compositions in the Fujian coastal area of SE China. The data used in this histogram are presented in Table B.2.

about 5%–10% biotite, and 22% of these also contain 5%–10% amphibole (Table B.2). In contrast, the Late Cretaceous granites show a lack of hydrous minerals, with <3%–5% (or even <1%) biotite, and only rare amphibole (Table B.2), implying a decrease of H_2O content in the younger magmas. Alternatively, the rare amphibole might be ascribed to the relatively lower CaO contents in the Late Cretaceous granites (average 1.18 wt%, $n = 84$; Tables A.2 and B.3) than those in the Early Cretaceous granites (average 3.98 wt%, $n = 42$; Tables A.2 and B.3), as the stability of amphibole seems to decrease with decreasing calcium composition in granitic systems (Naney, 1983). Yet, more importantly, the Late Cretaceous granites exhibit more significant negative Eu anomalies in their REE patterns than those of the Early Cretaceous granites (Fig. A.4), thus indicating a higher proportion of plagioclase crystallization in the hotter and less wet Late Cretaceous granitic magmas (Bachmann and Bergantz, 2008). Also, the Early Cretaceous I-type granites generally coexist with amphibole-bearing gabbros that typically contain considerable amounts of amphibole (generally 15%–55%; Table B.2). Mafic enclaves similar to the latter are generally produced by crystallization of relatively hydrous basaltic magmas (X. Xu et al., 1999), thus the presence of these gabbros implies a highly-hydrated Early Cretaceous mantle in this region. In contrast, H_2O-rich mafic intrusions were absent in the Late Cretaceous, whereas "anhydrous" A-type granites formed at 98–86 Ma in the area (Fig. 8). Furthermore, an increase of estimated magma temperature after ca. 100 Ma is supported by the increased zircon saturation temperatures of the Late Cretaceous I- and A-type granites (Fig. 9a). Such a change coincides with a decrease in water contents within their parental magma (e.g., Weinberg and Hasalová, 2015).

The Hf–Nd–O isotopes of the Early and Late Cretaceous plutonic rocks also display systematic changes over time (Figs. 9 and 10). More attention has been paid to the *in situ* zircon isotopes in these rocks, because zircon crystallizes relatively early in the evolution of a magma, and because it functions as a "tape recorder" that tracks details of Hf–O isotopic variations during magma evolution and is resistant to post-emplacement hydrothermal alteration (e.g., Griffin et al., 2002; Wei et al., 2002, 2008; Yang et al., 2007). Most Early Cretaceous rocks formed at 122–101 Ma along the Fujian coast have a large range of positive zircon $\varepsilon_{Hf}(t)$ values, whereas 80% of the younger Late Cretaceous granitoids contain a high proportion of zircon grains with negative $\varepsilon_{Hf}(t)$ values (most samples have >85% of grains with negative initial $\varepsilon_{Hf}(t)$ values). In particular, the Early Cretaceous I-type granites have generally positive zircon $\varepsilon_{Hf}(t)$ values with the average changing from +5.1 to −0.6 over 21 Ma (one exception being the 119 Ma Changqiao granite; Qiu et al., 2012). Such juvenile zircon Hf isotope features are comparable to those found in the Early Cretaceous gabbros, with the average $\varepsilon_{Hf}(t)$ value of individual gabbroic intrusions ranging from +8.2 to −1.5. In contrast with the Early Cretaceous granites, the vast majority of the younger Late Cretaceous granitoids (with the exception of the 87 Ma Zaoshan I-type pluton; Chen et al., 2014) display more negative average zircon $\varepsilon_{Hf}(t)$ values ranging from +1.1 to −5.4 for the I-types and from −1.3 to −3.0 for the A-types.

Moreover, the whole-rock Nd and zircon Hf isotopic compositions of the Cretaceous I- and A-type granites in the Fujian coastal area form a covariant array (Fig. A.5), basically paralleling the "initial Terrestrial Array" (Vervoort et al., 2011). This indicates the lack of Nd–Hf isotope decoupling in these granitoids. Therefore, the change in zircon $\varepsilon_{Hf}(t)$ values in the younger Late Cretaceous granites (Fig. 9b) is duplicated by their whole-rock Nd isotope compositions. On the $\varepsilon_{Nd}(t)$ vs. age diagram (Fig. 9c), the I- and A-type granites throughout the Cretaceous basically define a consistent evolution towards less-radiogenic Nd isotope compositions, especially during the Late Cretaceous.

Importantly, the compiled zircon O dataset also shows distinctive changes between the Early and Late Cretaceous granitoids, despite the limited amount of available data. As shown in Fig. 10, zircon grains in granite with ages from 117 to 116 Ma have $\delta^{18}O$ values lower than the typical mantle value of 5.3‰ (Valley et al., 2005), and a high proportion of grains plot significantly below the range of mantle-like values. These zircon grains are generally characterized by juvenile Hf isotopes with $\varepsilon_{Hf}(t)$ values mostly >0 (up to +3.1, Table B.4). Depletion of ^{18}O is usually attributed to the presence of high-temperature hydrothermally-altered igneous rocks in the source region (Bindeman et al., 2005; Bindeman and Simakin, 2014). Furthermore, positive zircon $\varepsilon_{Hf}(t)$ values in granites indicate the juvenile nature of the source region. Thus, the coupled feature of depletion of ^{18}O and juvenile Hf isotopes appears to require remelting of hydrothermally-altered oceanic crust (Bindeman et al., 2005; Wei et al., 2002). Conversely, zircon grains from granites with ages of 105–98 Ma are characterized by mantle-like $\delta^{18}O$ (Fig. 10), although about 67% of zircon grains (those grains with combined Hf–O isotopic data) show negative $\varepsilon_{Hf}(t)$ values. Whole-rock Re–Os and Sm–Nd isotopes of Early Cretaceous basaltic magmas from the SE China coastal region indicate high $\gamma_{Os}(t)$ values of +21.4 to +267.8, and $\varepsilon_{Nd}(t)$ values up to +2.7 (e.g., J.C. Zhou et al., 2006). Similarly, whole-rock Lu–Hf isotopes of ca. 88 Ma basaltic magmas in the region record positive $\varepsilon_{Hf}(t)$ values of +4.8 to +5.1 (e.g., Chen et al., 2014). These results suggest asthenosphere upwelling and a predominantly depleted mantle source along the SE China coast at this time. Recent studies on source lithologies of Mesozoic basalts in SE China also suggest a similar depleted asthenospheric mantle source (Zeng et al., 2016). Thus, the co-existence of evolved and juvenile Hf isotopes may reflect the involvement of evolved crustal components and melting of depleted mantle-derived underplated mafic rocks. Furthermore, the mantle-like $\delta^{18}O$ values may imply that their parental magmas were generated in environments devoid of hydrothermal alteration (possibly in the lower to middle crust). Regardless of the exact origin, extra heat from the underlying mantle is required in order for partial melting of deep-crustal (underplated) mafic rocks to occur. Zircon grains from the 87 Ma Zaoshan I-type granite are characterized by juvenile Hf isotopes and, importantly, a large range of $\delta^{18}O$ values varying from 6.3‰ to 3.5‰ (Chen et al., 2014; Table B.4 and Fig. 10). Such O isotope diversity in zircon grains is a typical characteristic of rift-related felsic volcanics (Bindeman and Simakin, 2014, and references therein), and could reflect the reworking and/or recycling of crustal igneous rocks in a continental rift environment with high thermal gradients (Wei et al., 2008), including recycling of high-temperature hydrothermally altered rhyolite to generate low-$\delta^{18}O$ magmas as proposed by Bindeman and Simakin (2014). Therefore, the systematic changes in Hf–O isotopes not only reflect the nature of the source region, but may also reveal additional information about the regional thermal state.

To conclude, currently-available data demonstrate the distinctive petrological and geochemical features of the Early and Late Cretaceous granitoids of Fujian Province in SE China. The high H_2O

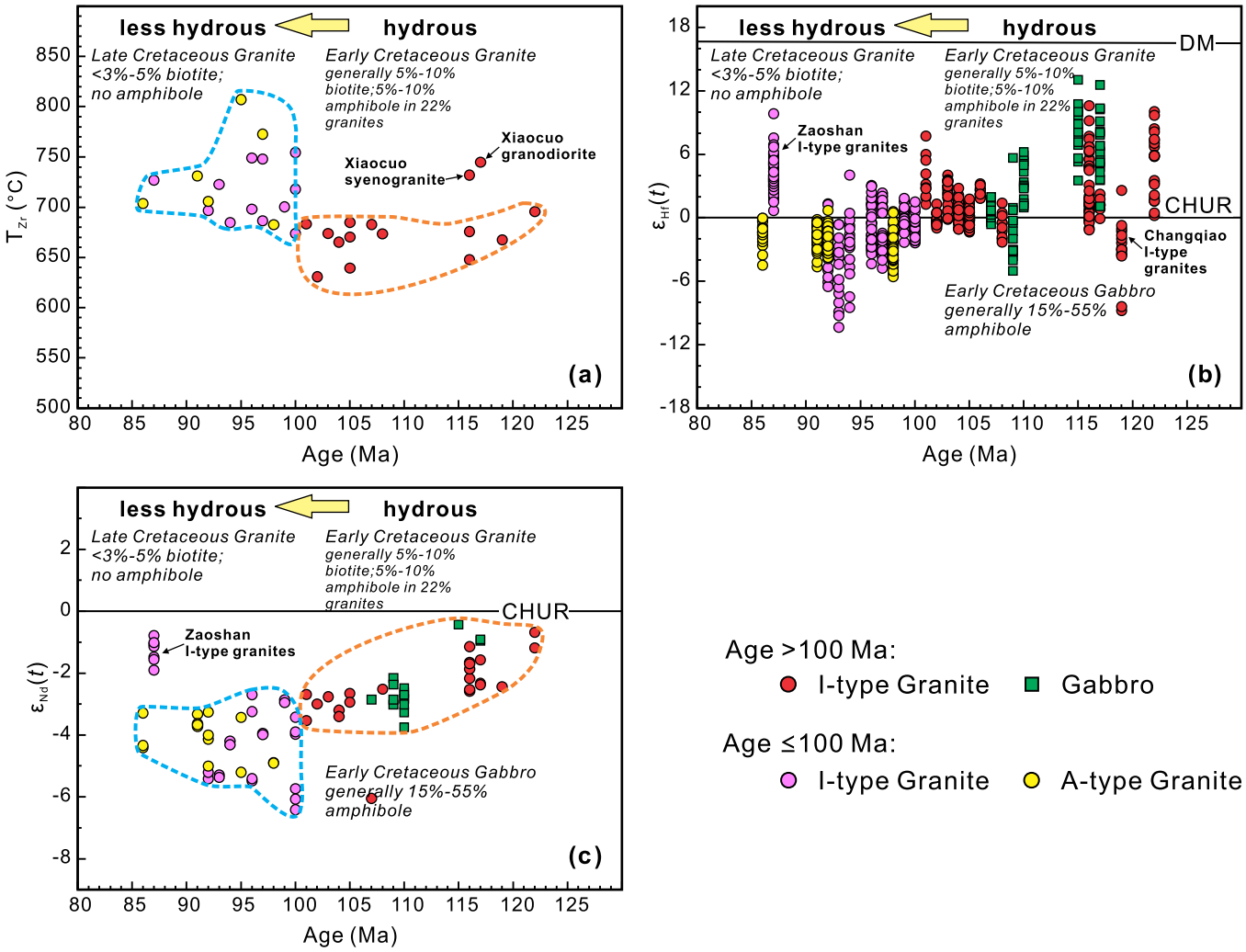

Fig. 9. (a) Zircon saturation temperature vs. U–Pb age diagram for Cretaceous granites in the Fujian coastal area of SE China. The average zircon saturation temperatures and ages of the Cretaceous plutons and batholiths are presented in Table B.2. The zircon saturation temperatures for the 117–116 Ma Xiaocuo granodiorite and syenogranite could be overestimated and imply the upper limit of magma temperatures, because zircon xenocrysts were present in these rock samples (Li et al., 2015). (b) $\varepsilon_{Hf}(t)$ vs. U–Pb age of igneous zircon grains from Cretaceous plutons and batholiths in the Fujian coastal area of SE China. The data are given in Table B.4. (c) $\varepsilon_{Nd}(t)$ vs. age diagram for Cretaceous plutons and batholiths in the Fujian coastal area of SE China. The data are given in Tables A.3 and B.3.

contents within the parental magmas of the Early Cretaceous granitoids, including the Pingtan and Tong'an granites, suggest that water-fluxed melting could be an important mechanism driving regional granitic magmatism. In the Late Cretaceous, water contents in the parental magmas of the granites along the Fujian coast decreased, and notably, this variation coincides with a change in the Hf–Nd–O isotopic systematics of these rocks.

6.3. Deep-Earth water cycling and continental crustal growth

We have shown that water (and/or other hydrous fluids) played a significant role in producing the Cretaceous granites within the coastal area of Fujian Province. Hence, identifying a mechanism by which water-fluxed melting can generate large-scale granitic magmatism is crucial for understanding the Cretaceous tectono-magmatic evolution of SE China. Answers to the following questions are prerequisites for identifying such a mechanism. For instance, what and where was the exact origin of the H_2O involved in crustal melting? How could the variation of Hf–Nd–O isotopes in granites be connected to a change in the H_2O contents of their parental magmas?

6.3.1. Shallow dehydration and partial melting of the subducted slab?

To understand the origin of the H_2O involved in crustal melting, as well as the processes that controlled the linkage between the magma H_2O contents and Hf–Nd–O isotopes of the Cretaceous granites along the Fujian coast, it is necessary to highlight the first-order observations on the late Mesozoic regional tectono-magmatic evolution in SE China. Late Mesozoic magmatism here is generally ascribed to the subduction of the Paleo-Pacific Plate beneath the Eurasian continent (e.g., Jahn et al., 1990; Zhou and Li, 2000). Jurassic–Cretaceous accretionary prisms/complexes and coeval forearc basins were identified along the Median Tectonic Line in Japan (MTL; line 1 in the upper left inset of Fig. 1a) (Takashima et al., 2004; Takasu and Dallmeyer, 1990). Furthermore, a Cretaceous high-temperature, but low-pressure, metamorphic belt (named the Tailuge belt) occurs on the eastern flank of the Central Ranges of Taiwan, China (line 2 in the upper left inset of Fig. 1a) (Zhou and Li, 2000, and references therein). Evidence for a coeval trench setting was also found in the Yuli belt of Taiwan (Zhou and Li, 2000, and references therein). Consequently, the possible paleo-suture zone was located approximately along the MTL in Japan (present coordinates; see Fig. 1a, upper left inset), and extending southwestwards to the eastern flank of the Central Ranges in Taiwan, China (Li et al., 2012, 2014).

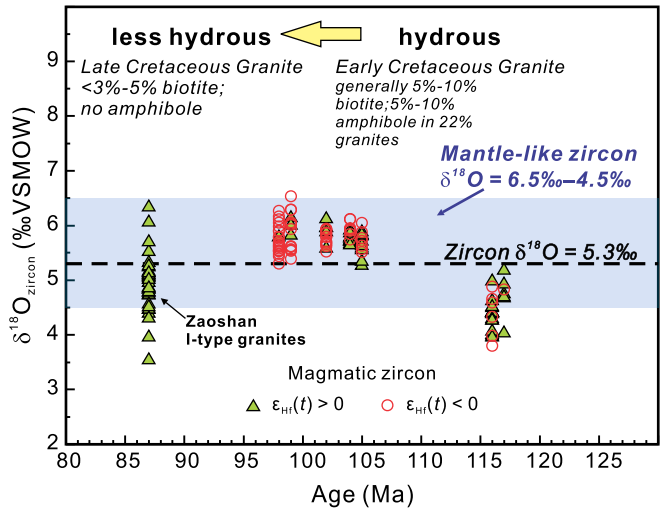

Fig. 10. *In situ* zircon $\delta^{18}O$ vs. U–Pb age diagram for Cretaceous granitoids in the Fujian coastal area of SE China. The diagram also shows the Hf isotope compositions of analyzed zircon grains (triangles, zircon grains with $\varepsilon_{Hf}(t) > 0$; circles, zircon grains with $\varepsilon_{Hf}(t) < 0$). VSMOW, Vienna standard mean ocean water. The data used in this diagram are given in Table B.4.

Interpretation of the petrogenesis of the late Mesozoic igneous rocks in SE China and their associated geodynamic setting generally involves subduction with variable angles of dip (e.g., X.M. Zhou et al., 2006; Zhou and Li, 2000), or flat-slab subduction (e.g., Li and Li, 2007). Moreover, the mechanism of slab rollback has been proposed for the late Mesozoic geodynamic environment in SE China (e.g., Li et al., 2007; Li and Li, 2007). For example, based on geochronological and geochemical data for the Cretaceous Fujian granites and gabbro–granite complexes, Li et al. (2012, 2014) demonstrated the presence of Cretaceous slab rollback in the coastal region of Fujian.

In subduction zones, hydrated and altered oceanic slabs are returned to the mantle by subduction, where water/hydrous fluids and other volatiles will be released by metamorphic devolatilization of the slabs and enter the mantle sources of arc volcanoes and back-arc basins (e.g., Spandler and Pirard, 2013). Incorporation of water from the shallow dehydration of subducting slabs (we use 'shallow' here to distinguish them from the 'deep' dehydration of stagnant slabs within the mantle transition zone; see discussion below) will lower mantle viscosity and may thus facilitate shallow vigorous asthenosphere convection beneath the back-arc lithosphere (Honda and Saito, 2003). Hyndman et al. (2005) proposed that the lithospheric architecture in circum-Pacific arc-backarc systems could have resulted from circulation of hydrous mantle in the back-arc region (e.g., the Cascadia subduction zone and back-arc in North America). Such an argument is supported by three-dimensional (3D) kinematic modelling of mantle flow, in which both poloidal and toroidal mantle circulations were observed during the subduction process (e.g., Schellart, 2008).

However, the shallow dehydration of subducting slabs may not supply enough water to generate the massive crustal melting in the coastal area of SE China, as demonstrated by the following lines of evidence. Firstly, slab rollback could explain the local Cretaceous extensional basins (X.M. Zhou et al., 2006), and may also cause large-scale counter-flow currents in the mantle wedge to account for regional lithospheric thinning and asthenospheric upwelling (Li et al., 2012). Evidence from other subduction systems has revealed that H_2O and/or hydrous fluids derived from the underlying subducting slab occur mainly close to the trench (e.g., island arc areas; Handley et al., 2011), whereas the SCMB in SE China was located within a back-arc region about 400–500 km from the eastern flank of the Central Ranges in Taiwan (a speculated location for the suture zone of the Paleo-Pacific slab in the late Mesozoic; Fig. 1a, upper left inset) (Li et al., 2014; Zhou and Li, 2000). Only minor water and other volatiles produced by shallow dehydration/melting of the down-going slab would be transferred to back-arc basins (Spandler and Pirard, 2013). Secondly, although 3D fluid dynamic experiments of subduction simulations identified both poloidal flow and quasi-toroidal return flow toward the mantle wedge during trench retreat and slab rollback, none of the experiments ever showed rollback induced poloidal flow around the slab tip (Schellart, 2008). These observations are therefore inconsistent with the underplating of hydrous basaltic magmas and water-fluxed melting during regional magmatism in the Fujian coastal area, which is far from the inferred paleo-suture zone. Thirdly, although flat-slab subduction (Li et al., 2007; Li and Li, 2007) seems to be capable of reconciling these discrepancies, the intensive Early Jurassic mantle melting, the high proportion of asthenospheric mantle components in ca. 195 Ma basalts, and the 195–190 Ma bimodal volcanic rocks (e.g., Cen et al., 2016) are inconsistent with the presence of a 1000 km diameter flat slab just beneath the sub-continental lithospheric mantle in SE China. Even if flat subduction is applicable in the Mesozoic in SE China, the large-scale Jurassic anorogenic magmatism in the hinterland of SE China requires a much earlier slab break-off and foundering at ca 190–155 Ma (Li et al., 2007; Li and Li, 2007). Considering the obvious temporal-spatial differences, shallow dehydration/partial melting of such foundered slabs would fail to contribute H_2O and/or hydrous fluids required for Cretaceous magmatism in the coastal area of SE China.

Therefore, a more rigorous mechanism is required to explain the high heat flow (Chen et al., 2008), lithospheric thinning and asthenospheric upwelling (Li et al., 2012) along the SE China coast. We need to seek out an alternative, or at least an additional mechanism, to account for the supply of both H_2O and heat, and to explain the distinctive variation of Hf–Nd–O isotopes in the Cretaceous granitic magmas (Figs. 9 and 10).

6.3.2. Deep-Earth water cycling: a possible alternative or additional model

Despite release of water/hydrous fluids (possibly including hydrous melts) from subducting oceanic slabs into the mantle wedge, the slabs can still retain significant H_2O, CO_2, and other crustal components to sub-arc depths (depths greater than arc magma generation depths) (e.g., Hacker, 2008; Spandler and Pirard, 2013; Wang et al., 2016, and references therein). Hacker (2008) estimated the amount of H_2O carried in subducting slabs by calculating phase diagrams for subducting bulk rock compositions and rock fluxes for global subduction zones, and suggested that about 35% of the global H_2O subducted at trenches can reach sub-arc depths. Subsequently, van Keken et al. (2011) prepared a global compilation of the thermal structure of subduction zones, yielding similar results with one third of the bound H_2O in subducting slabs recycled to >230 km depth. Such slab water could even survive to greater depths within the lower crust or lithospheric mantle by formation of ultra-high pressure (UHP) hydrous phases (Schmidt and Poli, 2003); the water may also be transported into the deep mantle by nominally anhydrous minerals (such as omphacite and majorite in the subducting basaltic crust), eventually forming a hydrous mantle transition zone (MTZ) at depths between 410 and 660 km (Fukao et al., 2009). The presence of the water-enriched high-pressure phases wadsleyite and ringwoodite (with high H_2O storage capacity of 1–3 wt%) demonstrated that the MTZ could be a large water reservoir in the deep-Earth (Fukao et al., 2009; Kuritani et al., 2011; Niu, 2014; Wang et al., 2015). Moreover, both subducted metasediments and mafic crust (Spandler et al., 2010), as well as carbonate rich lithologies in the slabs (Liu et al., 2015), may be recycled back into the deeper mantle, at least as deep as the MTZ.

Notably, those deep-subducted slab components, including H_2O, CO_2, and other crustal components, may be mixed gradually into the ambient mantle in the MTZ, and finally resurface along with mantle upwelling and accompanied magmatism (e.g., Kjarsgaard et al., 2017; Spandler and Pirard, 2013; Wang et al., 2016, and references therein). For example, diamonds sourced from the MTZ were observed widely in podiform chromitites and peridotites from ophiolites (Das et al.,

2017). U–Pb ages of euhedral zircon grains and Re–Os isotopes of Ru–Os–Ir sulphides in Tibetan chromitites indicate the survival of zircon in the MTZ and its subsequent return to the near surface in oceanic crust (now ophiolite) (McGowan et al., 2015). Additionally, some Cenozoic basalts derived from the hydrous MTZ were identified in east China (Wang et al., 2015), demonstrating the recycling of slab components via subduction to the MTZ. Recently, a > 4000 km long kimberlite corridor in North America suggests mid-Cretaceous kimberlite magmatism was related to water-fluxed decompression melting of C-O-H-bearing peridotite in the MTZ (Kjarsgaard et al., 2017).

One of the prominent geophysical features of the mantle beneath eastern China is the presence of a stagnant hydrated Paleo-Pacific slab within the MTZ (e.g., Huang and Zhao, 2006). The sluggish pyroxene–garnet transformation (Nishi et al., 2013) and slab viscosity (Nakakuki and Mura, 2013) in the MTZ would enable the stagnant slab to reside here for over 100 Ma before collapsing. Furthermore, recent studies indicate that collapse of the stagnant Paleo-Pacific slab may have started at ca. 24–25 Ma (estimated by calculating the cumulative amount of total subduction within the MTZ based on regional geophysical tomography, and by considering the temporal distribution of volcanism; Wang et al., 2015). Consequently, the stagnation of the subducted Paleo-Pacific slab should have occurred no later than ca. 125 Ma. This is consistent with rollback of the Paleo-Pacific slab in the Cretaceous along the SE China coast (see Section 6.3.1), because slab rollback would strongly facilitate the stagnation of the subducted oceanic slabs within the MTZ (e.g., Niu, 2014). Since H_2O, CO_2, and other crustal components derived from the subducted slabs can reach the MTZ in subduction zones, it is possible that the stagnant Paleo-Pacific slab in eastern China contained a considerable proportion of hydrous phases.

The following lines of evidence further show that large-scale stagnant hydrated oceanic slabs within the MTZ would release water and hydrous fluids/melts to the upper mantle. Investigations of lead and oxygen isotopes and the chemical composition of late Cenozoic basalts (Kuritani et al., 2011; Wang et al., 2015), as well as magnesium and zinc isotopes of Mesozoic-Cenozoic basalts (Huang et al., 2015; Liu et al., 2016), suggest that volatiles (water + CO_2) released from the stagnant Pacific slabs strongly hydrated the upper mantle beneath eastern China from 120 to 110 Ma (or even earlier). Subduction of the Paleo-Pacific slab and its stagnation in the deep Earth would lead to lower temperatures relative to those in the ambient MTZ, hence the fluid phases released by stagnant slabs should have large water contents and lower densities than the ambient mantle minerals (Jing and Karato, 2012). Subsequently, positive buoyancy can be expected to lead to upward percolation of water and other hydrous fluids or mantle melts, as confirmed by discovery of oxidized majorite inclusions from the deep asthenosphere (from at least ~380 km depth) within an orogenic carbonatite in the Trans–North China Orogen in eastern China (Xu et al., 2017).

Therefore, we propose that the MTZ at 410–660 km depth possibly offers an alternative (or additional) H_2O supply to generate hydrous basaltic underplating and water-fluxed crustal melting in SE China. Analogous to the Late Cretaceous Southwest Pacific region (Schellart et al., 2006), rollback of the subducted Paleo-Pacific slab occurred since the Early Cretaceous in the coastal region of SE China. Slab rollback may not only result in the formation of the upper crustal extensional basins in SE China (X.M. Zhou et al., 2006), but also lead to return flow in the mantle wedge to induce regional lithosphere thinning and possibly asthenospheric upwelling (Li et al., 2012). Over time, the hydrated slab subducted and stagnated in the MTZ (Fig. 11), then released fluid (or supercritical fluid) that induced extensive wet upwelling located atop or within the MTZ beneath SE China (Wang et al., 2015, and references therein). Water and hydrous melts (or supercritical fluid) may have ponded at the base of the continental crust and later provided H_2O to trigger, or more likely facilitate the water-fluxed melting of previously-underplated mafic rocks (possibly derived from shallow partial melting of previous low-angle or flat subducted slabs, considering the arc-like signatures of these mafic rocks), leading to the production of granitic melts within the continental crust (Fig. 11a). Experimental studies demonstrate that addition of even small amounts of free water (1–2%) can produce voluminous granitic melts by melting of crustal rocks (Weinberg and Hasalová, 2015). Thus, the addition of small amounts of water into the crust was capable of producing the huge volumes of Cretaceous granitoids in Fujian Province (Fig. 1). To facilitate the separation and emplacement of granitic melts into the middle to upper crust in SE China, water-fluxed melting might have been rock buffered (Weinberg and Hasalová, 2015) to produce H_2O-undersaturated melts capable of upward migration. Mingling between the underplated mafic and crustal granitic melts occurred, as attested by the presence of enclaves in some granitoids (see Section 6.1).

Adding water/fluid phases from the stagnant slabs may not only promote the further upwelling of asthenospheric mantle beneath eastern China, similar to the "Great Hydration" event that occurred beneath the Colorado Plateau (Schulze et al., 2015), but was likely to cause instability of the lowermost part of the continental lithosphere (Windley et al., 2010). We thus speculate that the upward percolation of hydrous fluid (or supercritical fluid) contributed significantly to facilitate, or control, lithosphere thinning (Li et al., 2012) and the high Cretaceous geothermal gradient or high thermal input (Chen et al., 2008) in the back-arc region of SE China. Furthermore, deep-Earth water cycling may also provide an additional, or an alternative, mechanism for lithospheric thinning and asthenospheric upwelling during the Mesozoic-Cenozoic in the North China Craton (e.g., Wilde et al., 2003; Windley et al., 2010).

In this deep-Earth water cycling process, the contribution of recycled sediments from subducted oceanic slabs should be limited, although sediments could have been subducted to the lower part of the MTZ in some cases (Liu et al., 2015). Firstly, the sedimentary lithologies within hydrated oceanic slabs are generally characterized by unradiogenic Nd–Hf isotopes (except for Fe–Mn crusts and nodules; e.g., Handley et al., 2011) and high $\delta^{18}O$ values (up to 10‰–42‰; Eiler, 2001). Thus, an injection of a large volume of such sediments into the source region would not only decrease $\varepsilon_{Nd}(t)$ and $\varepsilon_{Hf}(t)$ values in the magma, but also significantly increase magma oxygen delta values, generating much higher zircon $\delta^{18}O$ values relative to the normal mantle value of 5.3 ± 0.6‰ (Valley et al., 2005); generally >6.5‰ (Cavosie et al., 2005). Therefore, if the large range of zircon $\varepsilon_{Hf}(t)$ values observed in the Cretaceous Fujian granites was mainly caused by mixing of normal mantle melts (or other derivative juvenile components) with partial melts of recycled sediments from subducted oceanic slabs, high-$\delta^{18}O$ values (>6.5‰) would be widely observed in zircon grains. However, the zircon O isotopes of the Cretaceous granitoids in the coastal area of Fujian Province have predominantly mantle-like or even lower values, precluding significant involvement of recycled sediments from hydrated oceanic slabs in the source region (Fig. 10). It is likely that a significant proportion of any potential sediments in the subducted oceanic slabs had already been scraped off, as suggested by a series of Jurassic–Cretaceous accretionary prisms/complexes identified along the Median Tectonic Line in Japan (the likely location of the suture zone during late Mesozoic subduction of the Paleo-Pacific slab; Fig. 1a, upper left inset) (Li et al., 2012, and references therein).

The presence of low zircon $\delta^{18}O$ values (as low as 3.9‰) and juvenile Nd–Hf isotopes in some of Early Cretaceous granitoids in Fujian Province (Figs. 9 and 10) implies that both fluid and melts released from the subducted Paleo-Pacific slab could be directly involved in the genesis of granitic magmas (Bindeman et al., 2005). Generally, hydrothermal alteration has little effect on Nd–Hf isotopic ratios of altered oceanic crust (Handley et al., 2011, and references therein). This is confirmed by the fact that altered basalts from the western Pacific possess indistinguishable Nd–Hf isotopes compositions when compared to unaltered Pacific mid-ocean ridge basalt (MORB) (Chauvel et al., 2009). Thus, juvenile Nd–Hf isotopes and lower zircon O isotope values than the typical mantle value (close to 5.3‰) in some of the Early Cretaceous granites suggest that their source region may contain a large proportion

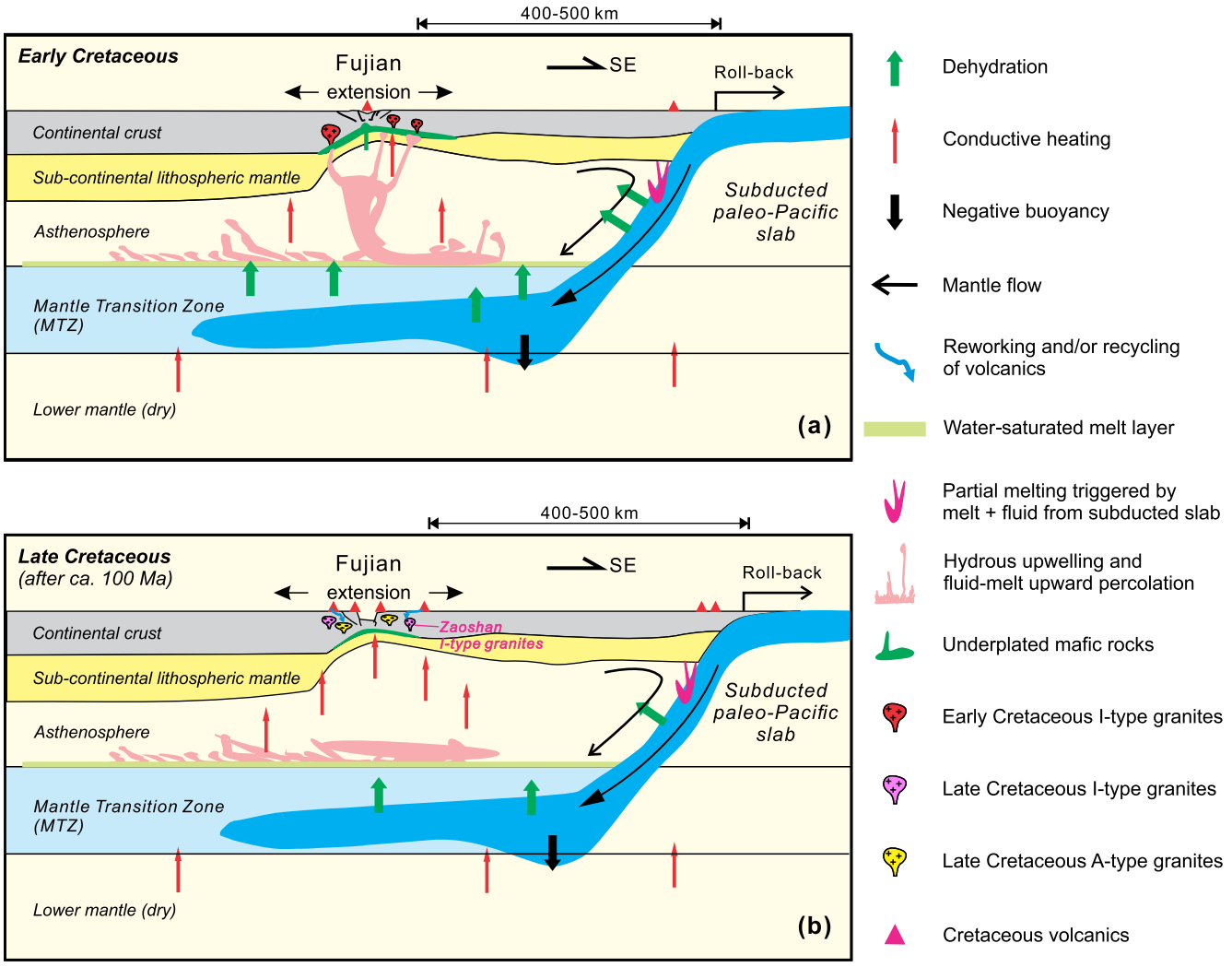

Fig. 11. Cartoon diagrams illustrating a possible water-fluxed melting model facilitated by deep-Earth water cycling to explain the Cretaceous tectono-magmatic evolution of the Fujian coastal area of SE China (modified after Wang et al., 2015). (a) Early Cretaceous scenario where intensive deep-Earth water cycling triggered by subduction and stagnation of the Paleo-Pacific slab may have induced massive wet upwelling to provide an alternative or additional H_2O supply to hydrous basaltic underplating and water-fluxed crustal melting beneath SE China that finally led to large-scale granitic magmatism. (b) Upward migration of water via wet upwelling decreased in the Late Cretaceous, whereas influx of heat from the mantle into continental crust remained high in this less-hydrous stage, due to continuous heat flow accompanying by asthenosphere upwelling (Chen et al., 2008). This would provide sufficient energy to result in the "hotter" Late Cretaceous A-type granites and voluminous felsic volcanics, along with reworking and/or recycling of evolved crustal components or some hydrothermally altered volcanics (possibly rhyolites) in the Late Cretaceous granitic magmas.

of components derived from Paleo-Pacific oceanic crust. Unfortunately, in this study we cannot determine the origin and proportions of these oceanic slab-derived melts. For example, were they derived from water-fluxed melting of previously-underplated mafic rocks? Was there any contribution from deep melting of the stagnant slab in the MTZ? Both the gabbroic and granitic rocks investigated here are intrusive rocks, which generally underwent complex crustal processes, such as crustal contamination, fractional crystallization, and magma mixing. Their primary source characteristics, whether attesting to deep melting or not, was probably obscured by the above-mentioned complex geological processes. Thus, further work is necessary to investigate the exact origin of the oceanic slab-derived melts.

Furthermore, the upward transport of hydrous fluid/melt via wet upwelling appears to have been reduced during the Late Cretaceous, possibly due to the decrease in supply of water following the decomposition/transformation of hydrous phases in the MTZ into anhydrous phases (Wang et al., 2015), and/or the increasing densities of any hydrous fluid/melt produced under higher temperatures (Jing and Karato, 2012). Following the decrease in wet upwelling, fewer oceanic crustal materials were involved in the genesis of the Late Cretaceous granites in Fujian Province. However, the influx of heat from the underlying mantle into the continental crust continued in this area, due to continuous heat flow accompanying asthenosphere upwelling (Fig. 11b) (Chen et al., 2008). Continued heat supply and its effect on the continental crust would provide energy to produce the "hotter" Late Cretaceous A-type granites (Chen et al., 2008) and felsic volcanics (e.g., Shimaoshan Formation; Guo et al., 2012) in Fujian, along with reworking and/or recycling of evolved crustal components and igneous rocks (e.g., hydrothermally altered rhyolite) in the generation of the Late Cretaceous felsic magma with diverse zircon $\delta^{18}O$ values (Bindeman and Simakin, 2014; Wei et al., 2008) (Figs. 10 and 11b). These observations demonstrate that deep-Earth water cycling could be an important mechanism that links the variation of Hf–Nd–O isotopes with change in magma H_2O contents in the Cretaceous granites along the Fujian coast.

7. Conclusions

We have presented petrographic, whole-rock geochemical and *in situ* zircon U–Pb and Lu–Hf isotopic data for mafic and felsic rocks

in the Pingtan and Tong'an complexes of Fujian Province in SE China. These results demonstrate the close spatial-temporal relationships and similar trace elemental and isotopic signatures between Cretaceous felsic and mafic magmas along the SE China coast. The juvenile Nd–Hf isotopic compositions of the granitic intrusions cannot be directly ascribed to massive mantle input. Hence, water-fluxed melting most likely contributed significantly to the complex geochemical features of these granites with juvenile isotopic compositions. Through combining our new data with the available published databases, we present a case that water-fluxed melting drove large-scale granitic magmatism, whereby the variation of magma H_2O contents coincided with a change in Hf–Nd–O isotopic characteristics. Our work demonstrates that rollback of the Paleo-Pacific slab and its shallow dehydration/partial melting in the subduction zone cannot alone directly account for the regional Cretaceous tectono-magmatic evolution. Deep-Earth water cycling provides an alternative (or additional) mechanism to supply H_2O and possibly other fluid phases for Cretaceous water-fluxed crustal melting in SE China, and also contributes to the underplating of hydrous basaltic magmas at the base of the crust, where they could later become mobilized and incorporated into subsequent intra-continental crustal differentiation. Deep-Earth water cycling also explains the variation of Hf–Nd–O isotopes and their coupling with change in magma H_2O contents. We therefore emphasize the link between deep-Earth water cycling and young continental crustal growth in eastern China, and note it may have a much wider global application.

Acknowledgements

We would like to thank Tao Yang, Lin-Hao Fang, Jia Wu and Ping Gao for their assistance with zircon U–Pb and Lu–Hf isotope analyses. Dr. William J. Collins is thanked for fruitful discussions and suggestions during an early phase of this study. We appreciate the thoughtful reviews and constructive suggestions provided by Dr. Ming Tang and an anonymous reviewer, and the helpful editorial advice of Dr. Xian-Hua Li. This work was supported by the National Natural Science Foundation of China (grant numbers 41302044, 41373033, 41602060), the Australian Research Council (ARC) Future Fellowship (FT140100826), the "Hundred Talents Program" of Shaanxi Province, China, the Science Foundation of Chang'an University (grant number 310827163412), and the Foundation of State Key Laboratory of Petroleum Resources and Prospecting (grant number PRP/open-1701).

Appendix A. Supplementary data

Supplementary data to this article can be found online at https://doi.org/10.1016/j.lithos.2017.12.028.

References

Bachmann, O., Bergantz, G.W., 2008. Rhyolites and their source mushes across tectonic settings. Journal of Petrology 49, 2277–2285.
Best, M.G., 2013. Igneous and metamorphic petrology. John Wiley & Sons.
Bindeman, I.N., Simakin, A.G., 2014. Rhyolites—hard to produce, but easy to recycle and sequester: integrating microgeochemical observations and numerical models. Geosphere 10, 930–957.
Bindeman, I., Eiler, J., Yogodzinski, G., Tatsumi, Y., Stern, C., Grove, T., Portnyagin, M., Hoernle, K., Danyushevsky, L., 2005. Oxygen isotope evidence for slab melting in modern and ancient subduction zones. Earth and Planetary Science Letters 235, 480–496.
Brown, M., 2001. Crustal melting and granite magmatism: key issues. Physics and Chemistry of the Earth, Part A: Solid Earth and Geodesy 26, 201–212.
Bureau of Geology and Mineral Resources of Fujian Province, 1998. Directions on Geological Map at Scale of 1:500000 of Fujian Province. Fujian Cartographic Publishing House, Fujian.
Campbell, I.H., Taylor, S.R., 1983. No water, no granites-no oceans, no continents. Geophysical Research Letters 10, 1061–1064.
Cavosie, A.J., Valley, J.W., Wilde, S.A., 2005. Magmatic $\delta^{18}O$ in 4400–3900 Ma detrital zircons: a record of the alteration and recycling of crust in the Early Archean. Earth and Planetary Science Letters 235, 663–681.
Cen, T., Li, W.X., Wang, X.C., Pang, C.J., Li, Z.X., Xing, G.F., Zhao, X.L., Tao, J., 2016. Petrogenesis of early jurassic basalts in southern Jiangxi Province, South China: implications for the thermal state of the Mesozoic mantle beneath South China. Lithos 256, 311–330.
Chappell, B., White, A., 1974. Two contrasting granite types. Pacific Geology 8, 173–174.
Chauvel, C., Marini, J.C., Plank, T., Ludden, J.N., 2009. Hf-Nd input flux in the Izu-Mariana subduction zone and recycling of subducted material in the mantle. Geochemistry, Geophysics, Geosystems 10, Q01001. https://doi.org/10.1029/2008GC002101.
Chen, C.-H., Lee, C.-Y., Lu, H.-Y., Hsieh, P.-S., 2008. Generation of Late Cretaceous silicic rocks in SE China: age, major element and numerical simulation constraints. Journal of Asian Earth Sciences 31, 479–498.
Chen, J.Y., Yang, J.H., Zhang, J.H., Sun, J.F., 2014. Geochemical transition shown by Cretaceous granitoids in southeastern China: implications for continental crustal reworking and growth. Lithos 196, 115–130.
Chen, M., Sun, M., Buslov, M.M., Cai, K., Zhao, G., Kulikova, A.V., Rubanova, E.S., 2016. Crustal melting and magma mixing in a continental arc setting: evidence from the Yaloman intrusive complex in the Gorny Altai terrane, Central Asian Orogenic Belt. Lithos 252, 76–91.
Clemens, J., Watkins, J.M., 2001. The fluid regime of high-temperature metamorphism during granitoid magma genesis. Contributions to Mineralogy and Petrology 140, 600–606.
Cogley, J.G., 1984. Continental margins and the extent and number of the continents. Reviews of Geophysics 22, 101–122.
Collins, W.J., Huang, H.Q., Jiang, X., 2016. Water-fluxed crustal melting produces Cordilleran batholiths. Geology 44, 143–146.
Das, S., Basu, A.R., Mukherjee, B.K., 2017. In situ peridotitic diamond in Indus ophiolite sourced from hydrocarbon fluids in the mantle transition zone. Geology 45, 755–758.
Eiler, J.M., 2001. Oxygen isotope variations of basaltic lavas and upper mantle rocks. Reviews in Mineralogy and Geochemistry 43, 319–364.
Fukao, Y., Obayashi, M., Nakakuki, T., Deep Slab Project Group, 2009. Stagnant slab: a review. Annual Review of Earth and Planetary Sciences 37, 19–46.
Griffin, W., Wang, X., Jackson, S., Pearson, N., O'Reilly, S.Y., Xu, X., Zhou, X., 2002. Zircon chemistry and magma mixing, SE China: in-situ analysis of Hf isotopes, Tonglu and Pingtan igneous complexes. Lithos 61, 237–269.
Guo, F., Fan, W., Li, C., Zhao, L., Li, H., Yang, J., 2012. Multi-stage crust–mantle interaction in SE China: temporal, thermal and compositional constraints from the Mesozoic felsic volcanic rocks in eastern Guangdong–Fujian provinces. Lithos 150, 62–84.
Hacker, B.R., 2008. H_2O subduction beyond arcs. Geochemistry, Geophysics, Geosystems 9, Q03001. https://doi.org/10.1029/2007GC001707.
Handley, H.K., Turner, S., Macpherson, C.G., Gertisser, R., Davidson, J.P., 2011. Hf–Nd isotope and trace element constraints on subduction inputs at island arcs: limitations of Hf anomalies as sediment input indicators. Earth and Planetary Science Letters 304, 212–223.
Hawkesworth, C., Dhuime, B., Pietranik, A., Cawood, P., Kemp, A., Storey, C., 2010. The generation and evolution of the continental crust. Journal of the Geological Society 167, 229–248.
Hier-Majumder, S., Tauzin, B., 2017. Pervasive upper mantle melting beneath the western US. Earth and Planetary Science Letters 463, 25–35.
Honda, S., Saito, M., 2003. Small-scale convection under the back-arc occurring in the low viscosity wedge. Earth and Planetary Science Letters 216, 703–715.
Hsieh, P.-S., Chen, C.-H., Yang, H.-J., Lee, C.-Y., 2008. Petrogenesis of the Nanling Mountains granites from South China: constraints from systematic apatite geochemistry and whole-rock geochemical and Sr–Nd isotope compositions. Journal of Asian Earth Sciences 33, 428–451.
Huang, J.L., Zhao, D.P., 2006. High-resolution mantle tomography of China and surrounding regions. Journal of Geophysical Research - Solid Earth 111, B09305. https://doi.org/10.1029/2005JB004066.
Huang, J., Li, S.-G., Xiao, Y., Ke, S., Li, W.-Y., Tian, Y., 2015. Origin of low $\delta^{26}Mg$ Cenozoic basalts from South China Block and their geodynamic implications. Geochimica et Cosmochimica Acta 164, 298–317.
Hyndman, R.D., Currie, C.A., Mazzotti, S.P., 2005. Subduction zone backarcs, mobile belts, and orogenic heat. GSA Today 15, 4–10.
Irvine, T., Baragar, W., 1971. A guide to the chemical classification of the common volcanic rocks. Canadian Journal of Earth Sciences 8, 523–548.
Jahn, B.M., Zhou, X.H., Li, J.L., 1990. Formation and tectonic evolution of southeastern China and Taiwan: isotopic and geochemical constraints. Tectonophysics 183, 145–160.
Jahn, B.M., Wu, F., Chen, B., 2000. Granitoids of the Central Asian Orogenic Belt and continental growth in the Phanerozoic. Geological Society of America Special Papers 350, 181–193.
Jing, Z., Karato, S.-I., 2012. Effect of H_2O on the density of silicate melts at high pressures: Static experiments and the application of a modified hard-sphere model of equation of state. Geochimica et Cosmochimica Acta 85, 357–372.
Johnson, T.E., Brown, M., Gardiner, N.J., Kirkland, C.L., Smithies, R.H., 2017. Earth's first stable continents did not form by subduction. Nature 543, 239–242.
Kemp, A.I.S., Hawkesworth, C.J., Collins, W.J., Gray, C.M., Blevin, P.L., 2009. Isotopic evidence for rapid continental growth in an extensional accretionary orogen: the Tasmanides, eastern Australia. Earth and Planetary Science Letters 284, 455–466.
Kjarsgaard, B.A., Heaman, L.M., Sarkar, C., Pearson, D.G., 2017. The North America mid-Cretaceous kimberlite corridor: Wet, edge-driven decompression melting of an OIB-type deep mantle source. Geochemistry, Geophysics, Geosystems 18, 2727–2747.
Kuritani, T., Ohtani, E., Kimura, J.-I., 2011. Intensive hydration of the mantle transition zone beneath China caused by ancient slab stagnation. Nature Geoscience 4, 713–716.
Li, Z.X., Li, X.H., 2007. Formation of the 1300-km-wide intracontinental orogen and postorogenic magmatic province in Mesozoic South China: a flat-slab subduction model. Geology 35, 179–182.

Li, X.H., Chung, S.L., Zhou, H., Lo, C.H., Liu, Y., Chen, C.H., 2004. Jurassic intraplate magmatism in southern Hunan-eastern Guangxi: $^{40}Ar/^{39}Ar$ dating, geochemistry, Sr-Nd isotopes and implications for the tectonic evolution of SE China. Geological Society, London, Special Publications 226, 193–215.
Li, X.H., Li, Z.X., Li, W.X., Liu, Y., Yuan, C., Wei, G., Qi, C., 2007. U–Pb zircon, geochemical and Sr–Nd–Hf isotopic constraints on age and origin of Jurassic I-and A-type granites from central Guangdong, SE China: a major igneous event in response to foundering of a subducted flat-slab? Lithos 96, 186–204.
Li, Z., Qiu, J.-S., Xu, X.-S., 2012. Geochronological, geochemical and Sr–Nd–Hf isotopic constraints on petrogenesis of Late Mesozoic gabbro–granite complexes on the southeast coast of Fujian, South China: insights into a depleted mantle source region and crust–mantle interactions. Geological Magazine 149, 459–482.
Li, Z., Qiu, J.-S., Yang, X.-M., 2014. A review of the geochronology and geochemistry of Late Yanshanian (Cretaceous) plutons along the Fujian coastal area of southeastern China: Implications for magma evolution related to slab break-off and rollback in the Cretaceous. Earth-Science Reviews 128, 232–248.
Li, Y., Ma, C.-Q., Xing, G.-F., Zhou, H.-W., Zhang, H., Brouwer, F.M., 2015. Origin of a Cretaceous low-^{18}O granitoid complex in the active continental margin of SE China. Lithos 216–217, 136–147.
Liu, L., Qiu, J.-S., Li, Z., 2013. Origin of mafic microgranular enclaves (MMEs) and their host quartz monzonites from the Muchen pluton in Zhejiang Province, Southeast China: Implications for magma mixing and crust–mantle interaction. Lithos 160-161, 145–163.
Liu, Y., He, D., Gao, C., Foley, S., Gao, S., Hu, Z., Zong, K., Chen, H., 2015. First direct evidence of sedimentary carbonate recycling in subduction-related xenoliths. Scientific Reports 5: 11547. https://doi.org/10.1038/srep11547.
Liu, S.A., Wang, Z.Z., Li, S.G., Huang, J., Yang, W., 2016. Zinc isotope evidence for a large-scale carbonated mantle beneath eastern China. Earth and Planetary Science Letters 444, 169–178.
Ma, Q., Xu, Y.G., Zheng, J.P., Griffin, W.L., Hong, L.B., Ma, L., 2016. Coexisting early Cretaceous high-Mg andesites and adakitic rocks in the North China Craton: the role of water in intraplate magmatism and cratonic destruction. Journal of Petrology 57, 1279–1308.
Maniar, P.D., Piccoli, P.M., 1989. Tectonic discrimination of granitoids. Geological Society of America Bulletin 101, 635–643.
McDonough, W.F., Sun, S.-S., 1995. The composition of the Earth. Chemical Geology 120, 223–253.
McGowan, N.M., Griffin, W.L., González-Jiménez, J.M., Belousova, E., Afonso, J.C., Shi, R., McCammon, C.A., Pearson, N.J., O'Reilly, S.Y., 2015. Tibetan chromitites: excavating the slab graveyard. Geology 43, 179–182.
Middlemost, E.A., 1994. Naming materials in the magma/igneous rock system. Earth-Science Reviews 37, 215–224.
Miller, C.F., McDowell, S.M., Mapes, R.W., 2003. Hot and cold granites? Implications of zircon saturation temperatures and preservation of inheritance. Geology 31, 529–532.
Nakakuki, T., Mura, E., 2013. Dynamics of slab rollback and induced back-arc basin formation. Earth and Planetary Science Letters 361, 287–297.
Naney, M.T., 1983. Phase equilibria of rock-forming ferromagnesian silicates in granitic systems. American Journal of Science 283, 993–1033.
Nishi, M., Kubo, T., Ohfuji, H., Kato, T., Nishihara, Y., Irifune, T., 2013. Slow Si–Al interdiffusion in garnet and stagnation of subducting slabs. Earth and Planetary Science Letters 361, 44–49.
Niu, Y.L., 2014. Geological understanding of plate tectonics: basic concepts, illustrations, examples and new perspectives. Global Tectonics and Metallogeny. 10, pp. 23–46.
Peccerillo, A., Taylor, S.R., 1976. Geochemistry of Eocene calc-alkaline volcanic rocks from the Kastamonu area, northern Turkey. Contributions to Mineralogy and Petrology 58, 63–81.
Petford, N., Gallagher, K., 2001. Partial melting of mafic (amphibolitic) lower crust by periodic influx of basaltic magma. Earth and Planetary Science Letters 193, 483–499.
Qiu, J.S., Li, Z., Liu, L., Zhao, J.L., 2012. Petrogenesis of the Zhangpu composite granite pluton in Fujian province: contraints from zircon U-Pb ages, elemental geochemistry and Nd-Hf isotopes. Acta Geologica Sinica 86, 561–576.
Schellart, W.P., 2008. Kinematics and flow patterns in deep mantle and upper mantle subduction models: Influence of the mantle depth and slab to mantle viscosity ratio. Geochemistry, Geophysics, Geosystems 9, Q03014. https://doi.org/10.1029/2007GC001656.
Schellart, W.P., Lister, G.S., Toy, V.G., 2006. A late Cretaceous and Cenozoic reconstruction of the Southwest Pacific region: tectonics controlled by subduction and slab rollback processes. Earth-Science Reviews 76, 191–233.
Schmidt, M.W., Poli, S., 2003. Generation of mobile components during subduction of oceanic crust. In: Rudnick, R. (Ed.), Treatise on Geochemistry. 3, pp. 567–591.
Schulze, D.J., Davis, D.W., Helmstaedt, H., Joy, B., 2015. Timing of the Cenozoic "Great Hydration" event beneath the Colorado Plateau: Th-Pb dating of monazite in Navajo volcanic field metamorphic eclogite xenoliths. Geology 43, 727–730.
Shen, W.Z., Zhu, J.C., Liu, C.S., Xu, S.J., Ling, H.F., 1993. Sm–Nd isotopic study of basement metamorphic rocks in south China and its constraint on material sources of granitoids. Acta Petrologica Sinica 9, 115–124.
Spandler, C., Pirard, C., 2013. Element recycling from subducting slabs to arc crust: a review. Lithos 170, 208–223.
Spandler, C., Yaxley, G., Green, D.H., Scott, D., 2010. Experimental phase and melting relations of metapelite in the upper mantle: implications for the petrogenesis of intraplate magmas. Contributions to Mineralogy and Petrology 160, 569–589.
Takashima, R., Kawabe, F., Nishi, H., Moriya, K., Wani, R., Ando, H., 2004. Geology and stratigraphy of forearc basin sediments in Hokkaido, Japan: Cretaceous environmental events on the north-west Pacific margin. Cretaceous Research 25, 365–390.
Takasu, A., Dallmeyer, R.D., 1990. $^{40}Ar/^{39}Ar$ mineral age constraints for the tectonothermal evolution of the Sambagawa metamorphic belt, central Shikoku, Japan: a Cretaceous accretionary prism. Tectonophysics 185, 111–139.
Tang, M., Wang, X.L., Shu, X.J., Wang, D., Yang, T., Gopon, P., 2014. Hafnium isotopic heterogeneity in zircons from granitic rocks: Geochemical evaluation and modeling of "zircon effect" in crustal anatexis. Earth and Planetary Science Letters 389, 188–199.
Tang, M., Chen, K., Rudnick, R.L., 2016. Archean upper crust transition from mafic to felsic marks the onset of plate tectonics. Science 351, 372–375.
Taylor, S.R., McLennan, S.M., 1995. The geochemical evolution of the continental crust. Reviews of Geophysics 33, 241–265.
Valley, J., Lackey, J., Cavosie, A., Clechenko, C., Spicuzza, M., Basei, M., Bindeman, I., Ferreira, V., Sial, A., King, E., 2005. 4.4 billion years of crustal maturation: oxygen isotope ratios of magmatic zircon. Contributions to Mineralogy and Petrology 150, 561–580.
van Keken, P.E., Hacker, B.R., Syracuse, E.M., Abers, G.A., 2011. Subduction factory: 4. Depth-dependent flux of H_2O from subducting slabs worldwide. Journal of Geophysical Research - Solid Earth 116:B01401. https://doi.org/10.1029/2010JB007922.
Vernon, R.H., Etheridge, M.A., Wall, V.J., 1988. Shape and microstructure of microgranitoid enclaves: indicators of magma mingling and flow. Lithos 22, 1–11.
Vervoort, J.D., Plank, T., Prytulak, J., 2011. The Hf–Nd isotopic composition of marine sediments. Geochimica et Cosmochimica Acta 75, 5903–5926.
Wang, P.Z., Chen, Y.A., Cao, B.T., Pan, J.D., Wang, C.Y., 1993. Crust–upper-mantle structure and deep structural setting of Fujian province. Geology of Fujian. 12, pp. 79–158.
Wang, X.C., Wilde, S.A., Li, Q.L., Yang, Y.N., 2015. Continental flood basalts derived from the hydrous mantle transition zone. Nature Communications 6, 7700.
Wang, X.C., Wilde, S.A., Xu, B., Pang, C.J., 2016. Origin of arc-like continental basalts: implications for deep-Earth fluid cycling and tectonic discrimination. Lithos 261, 5–45.
Waters, L.E., Lange, R.A., 2015. An updated calibration of the plagioclase-liquid hygrometer-thermometer applicable to basalts through rhyolites. American Mineralogist 100, 2172–2184.
Wei, C.-S., Zheng, Y.-F., Zhao, Z.-F., Valley, J.W., 2002. Oxygen and neodymium isotope evidence for recycling of juvenile crust in northeast China. Geology 30, 375–378.
Wei, C.-S., Zhao, Z.-F., Spicuzza, M.J., 2008. Zircon oxygen isotopic constraint on the sources of late Mesozoic A-type granites in eastern China. Chemical Geology 250, 1–15.
Weinberg, R.F., Hasalová, P., 2015. Water-fluxed melting of the continental crust: a review. Lithos 212, 158–188.
Whitney, J.A., 1988. The origin of granite: the role and source of water in the evolution of granitic magmas. Geological Society of America Bulletin 100, 1886–1897.
Wilde, S.A., Zhou, X., Nemchin, A.A., Sun, M., 2003. Mesozoic crust-mantle interaction beneath the North China craton: a consequence of the dispersal of Gondwanaland and accretion of Asia. Geology 31, 817–820.
Windley, B., Maruyama, S., Xiao, W., 2010. Delamination/thinning of sub-continental lithospheric mantle under Eastern China: the role of water and multiple subduction. American Journal of Science 310, 1250–1293.
Xia, S., Shen, Y., Zhao, D., Qiu, X., 2015. Lateral variation of crustal structure and composition in the Cathaysia block of South China and its geodynamic implications. Journal of Asian Earth Sciences 109, 20–28.
Xia, Q.K., Bi, Y., Li, P., Tian, W., Wei, X., Chen, H.L., 2016. High water content in primitive continental flood basalts. Scientific Reports 6:25416. https://doi.org/10.1038/srep25416.
Xu, X., Dong, C., Li, W., Zhou, X., 1999. Late Mesozoic intrusive complexes in the coastal area of Fujian, SE China: the significance of the gabbro-diorite–granite association. Lithos 46, 299–315.
Xu, X.S., Zhou, X.M., O'Reilly, S.Y., Tang, H., 1999. Exploration for the lower crustal materials and granite genesis in southeast China. Acta Petrologica Sinica 15, 217–223.
Xu, C., Kynický, J., Tao, R., Liu, X., Zhang, L., Pohanka, M., Song, W., Fei, Y., 2017. Recovery of an oxidized majorite inclusion from earth's deep asthenosphere. Science Advances 3, e1601589. https://doi.org/10.1126/sciadv.1601589.
Yang, J.H., Wu, F.Y., Wilde, S.A., Xie, L.W., Yang, Y.H., Liu, X.M., 2007. Tracing magma mixing in granite genesis: in situ U–Pb dating and Hf-isotope analysis of zircons. Contributions to Mineralogy and Petrology 153, 177–190.
Zeng, G., He, Z.Y., Li, Z., Xu, X.S., Chen, L.H., 2016. Geodynamics of paleo-Pacific plate subduction constrained by the source lithologies of Late Mesozoic basalts in southeastern China. Geophysical Research Letters:43 https://doi.org/10.1002/2016GL070346.
Zhou, X.M., Li, W.X., 2000. Origin of Late Mesozoic igneous rocks in Southeastern China: implications for lithosphere subduction and underplating of mafic magmas. Tectonophysics 326, 269–287.
Zhou, J.C., Jiang, S.Y., Wang, X.L., Yang, J.H., Zhang, M.Q., 2006. Re–Os isotopic compositions of late Mesozoic mafic rocks from southeastern coast of China. Acta Petrologica Sinica 22, 407–413.
Zhou, X.M., Sun, T., Shen, W.Z., Shu, L.S., Niu, Y.L., 2006. Petrogenesis of Mesozoic granitoids and volcanic rocks in South China: a response to tectonic evolution. Episodes 29, 26–33.